# Deglaciation of the highest mountains in Scandinavia at the Younger Dryas–Holocene transition: evidence from surface exposure-age dating of ice-marginal moraines

JOHN A. MATTHEWS [iD], HENRIETTE LINGE [iD], ATLE NESJE, PETER WILSON, RICHARD W. MOURNE, STEFAN WINKLER, GERAINT OWEN, JENNIFER L. HILL, STEFAN HASELBERGER AND JESPER OLSEN

**BOREAS**

Surface exposure–age dating was applied to rock surfaces associated with ice-marginal moraines at elevations of ~1520–1780 m a.s.l. on the slopes of Galdhøpiggen and Glittertinden, the two highest mountains in Scandinavia located in the Jotunheimen mountains of central southern Norway. This is important for understanding the pattern and timing of wastage of the Scandinavian Ice Sheet at the Younger Dryas–Holocene transition. Cosmogenic exposure dating (here $^{10}$Be dating) of boulders from the moraine ridges yielded overall mean ages (corrected for glacio-isostatic uplift, surface erosion and snow shielding) of ~11.6 ka from Galdhøpiggen and ~11.2 ka from Glittertinden. Similar $^{10}$Be ages were also obtained from additionally collected proximal and distal erratic boulders and bedrock samples. These enabled age calibration of Schmidt-hammer *R*-values and independent Schmidt-hammer exposure-age dating (SHD) of the moraine ridges, which yielded comparable mean SHD ages of ~10.8 and ~10.6 ka from the Galdhøpiggen and Glittertinden sites, respectively. Taking account of the age resolution and other limitations of both dating techniques, the results suggest that the two sets of moraines have approximately the same age but that neither technique can distinguish unambiguously between moraine formation in the late Younger Dryas or Early Holocene. Together with features of moraine-ridge morphology and estimates of equilibrium-line altitude depression of ~360–575 m (corrected for land uplift), the results imply moraine formation during short-lived re-advances of active glaciers, at least the lower reaches of which were warm-based. It is concluded that the local glaciers remained active and advanced during deglaciation either very late in the Younger Dryas or very early in the Holocene, possibly in response to the Preboreal Oscillation at ~11.4 ka. The study supports the concept of a thin Younger Dryas ice sheet and places time constraints on the timing of final deglaciation in southern Norway.

*John A. Matthews and Geraint Owen, Department of Geography, Swansea University, Singleton Park, Swansea SA2 8PP, Wales, UK; Henriette Linge (corresponding author: henriette.linge@uib.no) and Atle Nesje, Department of Earth Science, University of Bergen and Bjerknes Centre for Climate Research, NO-5020 Bergen, Norway; Peter Wilson, School of Geography and Environmental Sciences, Ulster University, Coleraine, Co. Londonderry BT52 1SA, Northern Ireland, UK; Richard W. Mourne, School of Architecture and Environment, University of the West of England, Coldharbour Lane, Bristol BS16 1QY, England, UK; Stefan Winkler, Department of Geography and Geology, Julius-Maximillians-University Würzburg, Am Hubland, D-9707 Würzburg, Germany; Jennifer L. Hill, Academic Development Unit, University of Gloucestershire, Cheltenham GL50 2RH, England, UK; Stefan Haselberger, Department of Geography and Regional Research, University of Vienna, Universitätstraße 7, 1010 Vienna, Austria; Jesper Olsen, Aarhus AMS Centre (AARAMS), Department of Physics and Astronomy, Aarhus University, 8000 Aarhus C, Denmark; received 28th May 2023, accepted 3rd December 2023.*

The Scandinavian Ice Sheet was the largest component of the interconnected complex of Eurasian ice sheets during the Last Glacial Cycle and its demise was completed by 9 ka (Hughes *et al.* 2016; Stroeven *et al.* 2016). Deglaciation involved both ice-margin retreat (backwasting) and surface lowering (downwasting/thinning), and the datable domain in both cases is the numeric timing of ice absence. Backwasting has been mapped and dated in multiple ways, as shown in the reviews of Nesje (2009) and Mangerud *et al.* (2011, 2023), and the data compilations and modelling of Cuzzone *et al.* (2016), Hughes *et al.* (2016) and Stroeven *et al.* (2016). Down-wasting, however, is more difficult to map in time and space as it requires dateable features of environmental change, such as landforms delineating inland ice margins and sedimentary archives of changing local conditions.

Whereas the horizontal limits of the Scandinavian Ice Sheet during the later phases of ice wastage in the Younger Dryas (12.9–11.7 ka) are generally well defined by ice-marginal moraines throughout the Scandinavian Peninsula and Finland, the vertical limits are much more difficult to define, especially away from the peripheral areas (Briner *et al.* 2014, 2023; Cuzzone *et al.* 2016; Hughes *et al.* 2016; Stroeven *et al.* 2016; Romundset *et al.* 2023). Hence, the ice thickness and surface geometry are poorly understood, conceptual models of deglaciation remain controversial and the evidential basis for modelling is incomplete. This is due largely to the lack of field evidence left by the cold-based ice in the interior areas of the ice sheet (Sollid & Sørbel 1988, 1994; Kleman & Hättestrand 1999; Kleman *et al.* 2008; Patton *et al.* 2017; Mangerud *et al.* 2023), and because large

tracts of these areas lay above the contemporaneous equilibrium-line altitude (ELA).

It is established that deglaciation was well underway throughout most of the Scandinavian Peninsula by the end of the Younger Dryas but this does not necessarily apply to the highest plateaus and mountains (Dahl *et al.* 1997; Goehring *et al.* 2008; Andersen *et al.* 2019; Marr *et al.* 2019; Lane *et al.* 2020; Briner *et al.* 2023; Romundset *et al.* 2023). Deglaciation at the Younger Dryas/Holocene transition in the inland areas of Scandinavia is generally considered to have been dominated by ice-sheet downwasting. This is seen as a response to rapid climatic warming at the Younger Dryas–Holocene transition, and the consequent rise in the ELA above the ice-sheet surface. Near the centre of a multidomed Younger Dryas ice sheet, downwasting appears to have resulted in extensive nunatak areas above the ice-sheet surface while stagnant ice masses survived in the adjacent valleys (Dahl *et al.* 1997; Linge *et al.* 2006; Goehring *et al.* 2008; Romundset *et al.* 2023). However, ice-marginal moraines on the high plateau of Dovrefjell in central Norway have been dated to the Younger Dryas (Lane *et al.* 2020) and appear to demonstrate the existence of active, warm-based ice at the margin of the retreating ice sheet at elevations up to ~1800 m a.s.l.

Chronological data defining the timing of the final deglaciation in the high-elevation areas near the centre of the Scandinavian Ice Sheet are sparse. Specific obstacles include: (i) a general lack of dateable depositional landforms at high-elevation sites affected by cold-based ice sheets; (ii) dependence of age estimates on radiocarbon dating of archives in which organic material is sparse and often non-representative of the timing of ice downwastage; and (iii) suboptimal environmental conditions for surface exposure dating using *in situ* cosmogenic nuclides (e.g. postdepositional boulder disturbance from periglacial activity). However, by providing the means to directly determine the timing of ice absence, surface exposure dating using *in situ* cosmogenic nuclides is now the main chronological tool for elucidating the retreat of past ice sheets and glaciers (Balco 2011, 2020).

In this paper, we focus on the age and significance of high-elevation ice-marginal moraines in Jotunheimen, southern Norway. The moraine ridges are located at elevations of up to ~1780 m a.s.l. on the two highest mountain massifs in Scandinavia (Fig. 1). At the maximum of the last (Weichselian) glaciation, the highest areas of Jotunheimen were located close to the main ice divide and ice accumulation area of the Scandinavian Ice Sheet (Vorren & Mangerud 2008; Mangerud *et al.* 2023). Our first objective was to establish the age
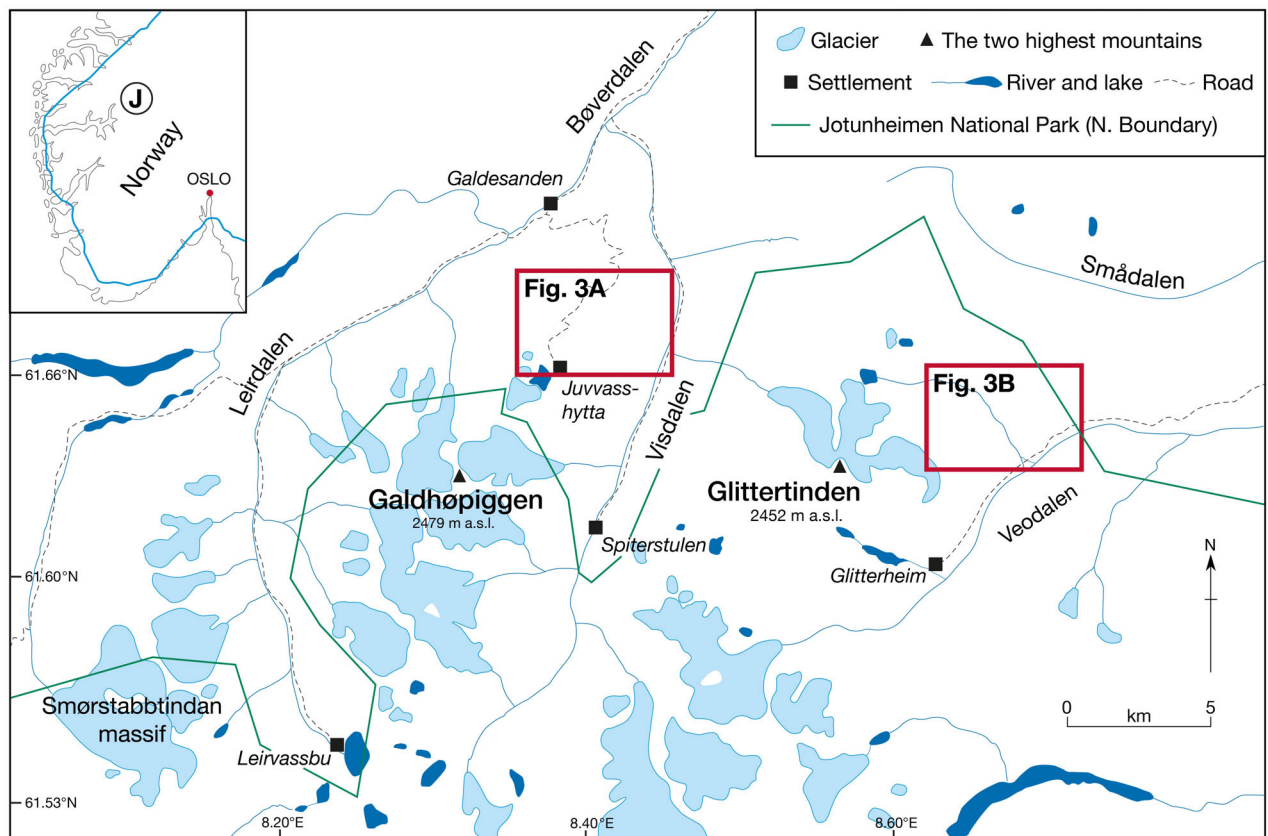


*Fig. 1.* Location map of the study areas. Inset map locates Jotunheimen (J) in southern Norway and the maximum extent of the Scandinavian Ice Sheet during the Younger Dryas Stadial (YD, blue line).

of the moraines using two complementary exposure-age dating techniques: [10]Be and Schmidt hammer exposure-age dating (SHD). The latter technique is used to provide independent, complementary age estimates that can be obtained relatively easily and non-destructively from a large sample of rock surfaces at the same sites (Matthews & Winkler 2022), allowing data to be collected with little or no disturbance of wildlife or compromise of the natural environmental, aesthetic, archaeological, historical or cultural value of the sites. The second objective was to reconstruct the ELA at the time of moraine-ridge deposition and hence to determine the equilibrium-line depression (ΔELA), which is indicative of the palaeoclimatic environment of the former glaciers relative to the present-day glaciers at these sites. The third objective was to summarize the results and implications in a conceptual model of deglaciation at the Younger Dryas–Holocene transition. In particular, we examine whether ice masses at the highest elevations could have persisted after the end of the Younger Dryas and expanded again in the Early Holocene. The identification and dating of high-elevation moraine ridges in Jotunheimen therefore provide potentially valuable contributions towards constraining the ice configuration in time and space, interpreting palaeoenvironmental information from glacial geomorphological evidence and updating models of deglaciation for high-elevation areas close to the centre of the Scandinavian Ice Sheet.

## Study area and environmental background

The study area includes the northern flanks of the two highest mountains in Scandinavia – Galdhøpiggen, 2469 m a.s.l. and Glittertinden, 2452 m a.s.l. – where moraine ridges were identified, mapped and sampled over an elevation range of ~1530–1780 m a.s.l. (Fig. 1). These sites are the only ones known to the authors with similar distinct moraine ridges at such high elevations in Jotunheimen. The landscape at and above this elevation is largely till covered with extensive areas of boulders, cobbles and disturbed soils, forming patterned ground and other periglacial landforms (Ødegård et al. 1987, 1988; Cook-Talbot 1991; Winkler et al. 2016, 2020, 2021; Matthews et al. 2019). The sparse alpine vegetation, dominated by grass and lichen heath with occasional dwarf shrubs and herbaceous perennials, is characteristic of the mid-alpine belt, the upper limit of which occurs locally at about 1600 m a.s.l. (Matthews et al. 2018; Hallang et al. 2022). The local bedrock is composed predominantly of pyroxene granulite gneiss, commonly with gabbroic textures, and less common mylonitized zones, peridotite outcrops and quartzitic veins (Battey & McRitchie 1973, 1975; Lutro & Tveten 2012).

Modelled weather data for the area, with a spatial and temporal resolution of 1 km and 24 h, are available via the online resource seNorge.no (http://www.senorge.no). Air temperature and precipitation data (Table S1) are calculated via spatial interpolation of point observations, while snow data are simulated with snow models using the weather data (Lussana et al. 2019). The mean annual air temperature (MAAT) for the climate normal period 1991–2020 is −3.1 °C at 1661 m a.s.l. and −2.6 °C at 1564 m a.s.l. for the Galdhøpiggen area, and −3.5 °C at 1645 m a.s.l. for the Glittertinden area. The corresponding lowest temperatures occur in February (−10.0, −9.6 and −11.1 °C, respectively) and the highest in July (6.3, 6.9 and 6.4 °C, respectively). Annual precipitation for the same period is 650, 664 and 932 mm, respectively, with a maximum in July and August. The late-summer maximum is characteristic of the continental climatic regime of eastern Norway. Modelled snow thickness shows an annual mean of 50 and 47 cm at the two elevations on Galdhøpiggen, and 43 cm at the Glittertinden site. Maximum snow depths of ~100 cm occur in April, whereas August is the only month without snow.

Present-day glaciers exist closely adjacent to the study sites at elevations down to ~1830 m a.s.l. (Veslgjuvbrean/-Galdhøpiggen) and ~1860 m a.s.l. (Gråsubrean/Glittertinden), respectively (Andreassen & Winsvold 2012; Andreassen 2022). Mountain permafrost is extensive in the area where the lower limits of continuous and discontinuous permafrost may extend down to ~1700 and ~1450 m a.s.l., respectively (Ødegård et al. 1992; Hauck et al. 2004; Farbrot et al. 2011; Lilleøren et al. 2012). Permafrost may be >300 m thick in the continuous permafrost zone at 1890 m a.s.l. (Isaksen et al. 2002). The present-day glaciers are therefore cold-based in their terminal zones (Etzelmüller et al. 2003; Etzelmüller & Hagen 2005) where the MAAT is approximately −4 °C. Glaciers and permafrost interact in the area to form characteristic ice-cored moraines close to present glacier margins (Østrem 1964, 1965; Lilleøren & Etzelmüller 2011; Matthews et al. 2014).

Based on climate proxies and modern climate–permafrost relationships Lilleøren et al. (2012) demonstrated that the altitudinal limits of permafrost in the Galdhøpiggen massif varied during the Holocene from about 200 m higher than today towards the end of the Holocene Thermal Maximum to about 200 m lower than today during the Little Ice Age. At the elevations of the moraines of interest in this study, permafrost is likely to have been absent during the Holocene Thermal Maximum. The lowest permafrost limits of the Late Holocene seem to have occurred during the Little Ice Age when the MAAT was ~1.0 °C lower than in AD 1961–1990 (Lilleøren et al. 2012). These variations in permafrost limits are generally coeval with glacier variations in the neighbouring Smørstabbtindan massif and elsewhere in southern Norway, where glaciers melted away during the Holocene Thermal Maximum, re-formed after ~6.0 ka (neoglaciation) and reached their Late Holocene maxima in the 18th century during the Little Ice Age (Matthews 1991, 2005, 2013; Matthews & Dresser 2008).

Matthews *et al.* (2014) obtained SHD ages of several thousand years from the very large multiple-ridged ice-cored moraine (Gråsuranden) in front of Gråsubrean, which rises >30 m above the surrounding terrain, and concluded that the moraine ridges were produced by sediment deformation resulting from Late Holocene glacier advances in the permafrost environment. The present form of the ice-cored moraine resulted from major reworking during the Little Ice Age, which was the last and most extensive centennial-scale glacier expansion episode of the Late Holocene in Jotunheimen.

Little evidence exists relating specifically to the timing of Lateglacial/Holocene deglaciation in the study area. According to the DATED-1 reconstruction, Jotunheimen was deglaciated after 10 ka (Hughes *et al.* 2016), but this is a low-resolution reconstruction that does not take adequate account of local topographic variation. Minimum estimates of deglaciation age from northern and eastern Jotunheimen based on radiocarbon-dated organic material from lakes and mires in low-alpine and sub-alpine locations are mostly in the range 9.5–10.5 cal. a BP (e.g. Nydal *et al.* 1970; Gunnarsdóttir 1996; Barnett *et al.* 2000; Matthews *et al.* 2000, 2005; Nesje & Dahl 2001; Matthews & Dresser 2008; Velle *et al.* 2010). These estimates are likely to have been influenced to varying degrees by delayed organic production in newly deglaciated landscapes. Velle *et al.* (2010) considered that deglaciation occurred in the Early Holocene (~11 cal. ka BP) at Brurskardstjønne in eastern Jotunheimen (1309 m a.s.l.) followed by rapidly increasing local organic production from about 10 ka. The oldest available radiocarbon date from Bukkehåmårtjørna (1594 m a.s.l.), eastern Jotunheimen, suggests that deglaciation may have occurred between 11.9 and 11.2 cal. ka BP (Lie *et al.* 2004). Periglacial patterned ground in the immediate vicinity of the moraines and on Juvflye indicates that peak frost sorting occurred during the Early Holocene and seems to have commenced shortly after deglaciation (Winkler *et al.* 2016, 2020), but precise dating was hampered by the lack of independent local old control points for SHD.

## Material and methods

### Moraine characteristics and mapping

This study focuses on relict ice-marginal moraine ridges that occur up to 2.5 km from today's glaciers (Figs 2, S1–S3). The ridges are composed of diamictons with abundant fines and a variable boulder component. They lack the characteristic morphology of the massive ice-cored moraine ramparts that lie much closer to the glaciers at a higher elevation. There is no evidence of the anastomosing ridges that are produced as a result of sediment deformation and creep associated with the ice-cored moraines formed by polythermal glaciers in a permafrost environment. Instead, they are smaller,

discrete ridges that rise 2–10 m above the surrounding terrain and are more typical of the moraines of temperate glacier landsystems produced by climatically induced advances or still-stands in the position of the glacier margin (cf. Evans 2003; Etzelmüller & Hagen 2005).

The moraine ridges were identified in the field and mapped with the aid of colour aerial photographic images from 23 September 2017 available with 0.25 m resolution from the Norge i bilder website (https://www.norgeibilder.no/). However, preservation of the moraines is poor in places because of widespread postdepositional paraglacial and periglacial activity, including gullying, solifluction (e.g. Fig. 2B) and the development of sorted patterned ground (circles and stripes). The landscape setting of the moraines is indicated in Figs S1 and S2.

At the site on Galdhøpiggen, segments of a single arcuate latero-terminal moraine ridge can be followed over a total distance of >2 km and an elevation range of ~1550–1620 m a.s.l. (Fig. 3A). Although the eastern lateral moraine is less well defined because of greater erosional activity on steeper slopes, well-preserved moraine fragments define the outline of the lower parts of a palaeoglacier. The minimum extent of this palaeoglacier is interpreted as a relatively small, isolated glacier located beneath the north-facing slope of a small hill, Juvvasshøe (1894 m a.s.l.), close to the northern edge of the high-elevation Juvflye plateau (Fig. 3A). The closest glacier, Juvfonne, is a small (~0.1 km$^2$) ice patch located >3 km to the SW, between 1852 and 1985 m a.s.l. (Kjøllmoen *et al.* 2021), and it has existed continuously since ~7600 cal. a BP (Ødegård *et al.* 2017). Today, the ice patch covers an area of about 0.086 km$^2$, and is a centre of attention for mass balance monitoring (Kjøllmoen *et al.* 2021) and findings of archaeological artefacts (Ødegård *et al.* 2017). An alternative interpretation of the maximum extent of the palaeoglacier is that it represents the extent of a merged Juvfonne/Kjelen/Veslejuvbrean palaeoglacier that expanded from the eastern side of Galdhøe (2223 m a.s.l.) onto the Juvflye plateau and overran Juvasshøe (Fig. 3A).

In the Glittertinden area, a moraine belt consists of two and in places more ridges, which is indicative of the margin of an expanded Gråsubrean palaeoglacier. The moraine ridges can be traced for >2 km across the mountainside SE of Glittertinden (Fig. 3B). This moraine belt is about 100 m wide at elevations of ~1520–1800 m a.s.l. At the highest elevations it is oriented NW–SE, approximately parallel and approximately 1 km distal to Gråsuranden, the ice-cored moraine of Gråsubrean. At lower elevations, the re-orientation of the moraine ridges towards the east indicates that ice from the palaeoglacier was confluent with a valley glacier flowing down Veodalen. The palaeoglacier can therefore be interpreted as representing an ice cap on Glittertinden. Further east, at an elevation of ~1500 m a.s.l., the moraine belt turns towards the NE, entering the lower part of the broad,
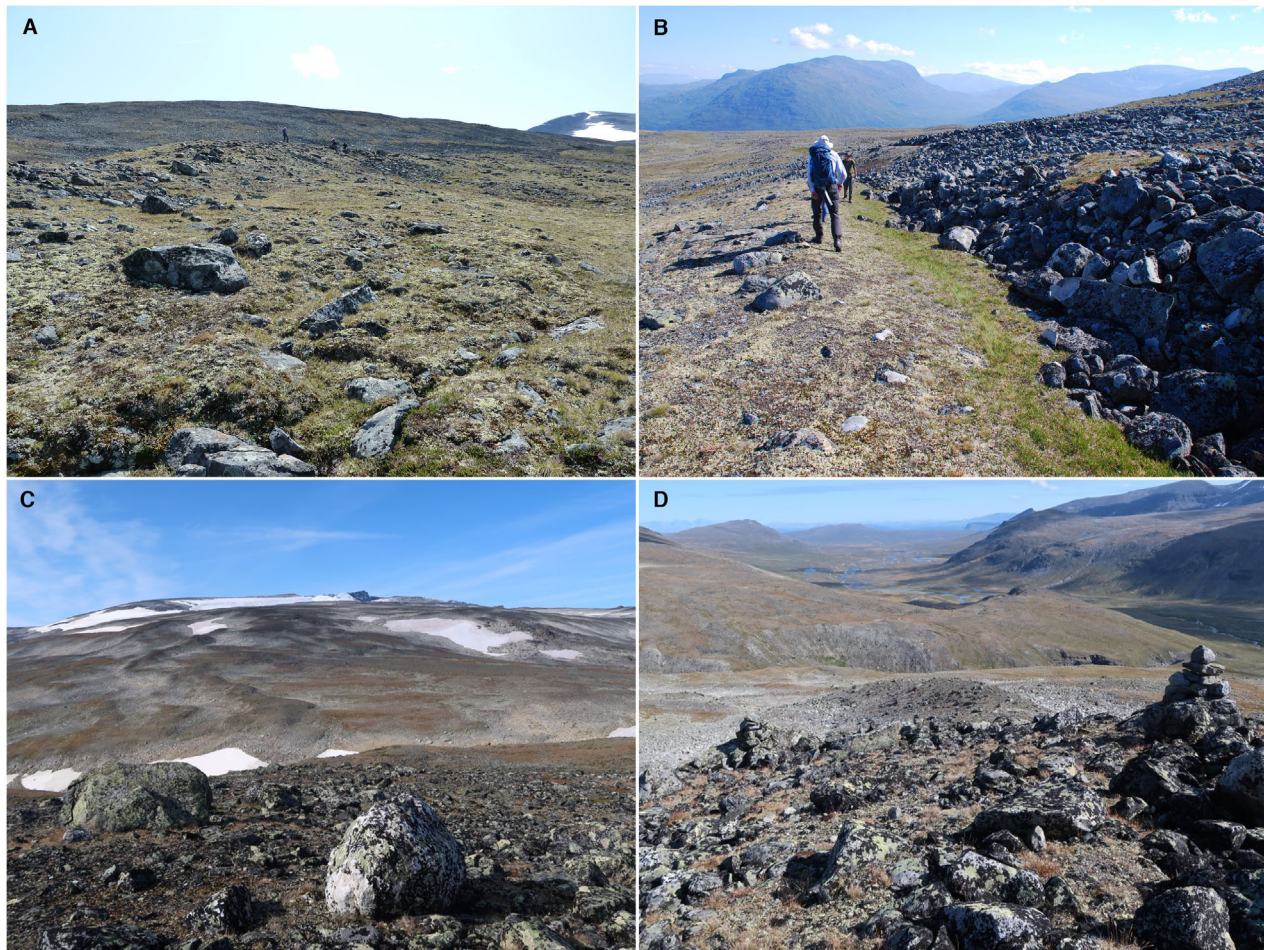
*Fig. 2.* Photographs of the moraine ridges dated using [10]Be and Schmidt-hammer exposure-age dating (SHD). A. The western ridge is from the Galdhøpiggen study area: note the scale from people standing on the ridge crest, which rises diagonally across the hillside towards the Juvfonne ice patch on the skyline. B. Uppermost part of the western ridge from the Galdhøpiggen study area close to the Galdhøpiggvegen road: note stone-banked solifluction lobes (left) abutting the proximal slope of the ridge, whereas the ridge crest appears unaffected by periglacial processes. C. The outer ridge of the moraine belt from the Glittertinden study area (viewed from the east side of the Bergenussa river valley) winds upslope towards Gråsubrean and Glittertinden on the skyline. D. Close up of the same ridge at the relatively high elevation of 1750 m a.s.l.

shallow valley of Trollsteinkvelven for a short distance of a few hundred metres. Four discrete ridges can be identified at this point. Moraine ridges are much less clear and could not be traced far to the east of the Bergenussa river.

*Sampling and material analysis for [10]Be dating*

At the Galdhøpiggen sites, samples were collected from moraine ridges and sites both 'inside' and 'outside' of the inferred limits of the local palaeoglaciers. Moraine-ridge sites are represented by seven boulder samples of granitic–granodioritic composition from western and eastern segments of the latero-terminal moraine (elevation range 1557–1566 m a.s.l.). A single bedrock surface of felsic composition from south of the moraine at an elevation of 1694 m a.s.l. represents the only 'inside' site, and it is used as a test for the presence of inheritance and hence whether the local palaeoglacier could have been

low-erosive and cold-based. Three 'outside' samples were taken from granulite erratics: two were embedded in till and one rested on exposed bedrock. They were located approximately 1 km south and east of the eastern moraine segment, within an elevation range of 1611–1636 m a.s.l. The sampling design was based on the hypothesis that surface exposure ages derived from the moraine samples would indicate the timing of moraine formation by the palaeoglacier, whereas ages from the 'outside' sites would potentially date an earlier phase of deposition relating to deglaciation of a more extensive ice cover.

At the Glittertinden sites, samples were taken from moraine ridges and 'inside' sites. Seven granulite boulders were sampled from the two most prominent ridges within the moraine belt (elevation range 1528–1759 m a.s.l.) while four 'inside' samples relate to granulite erratics on bedrock (two samples) or granulite veins in bedrock (two samples) at various elevations
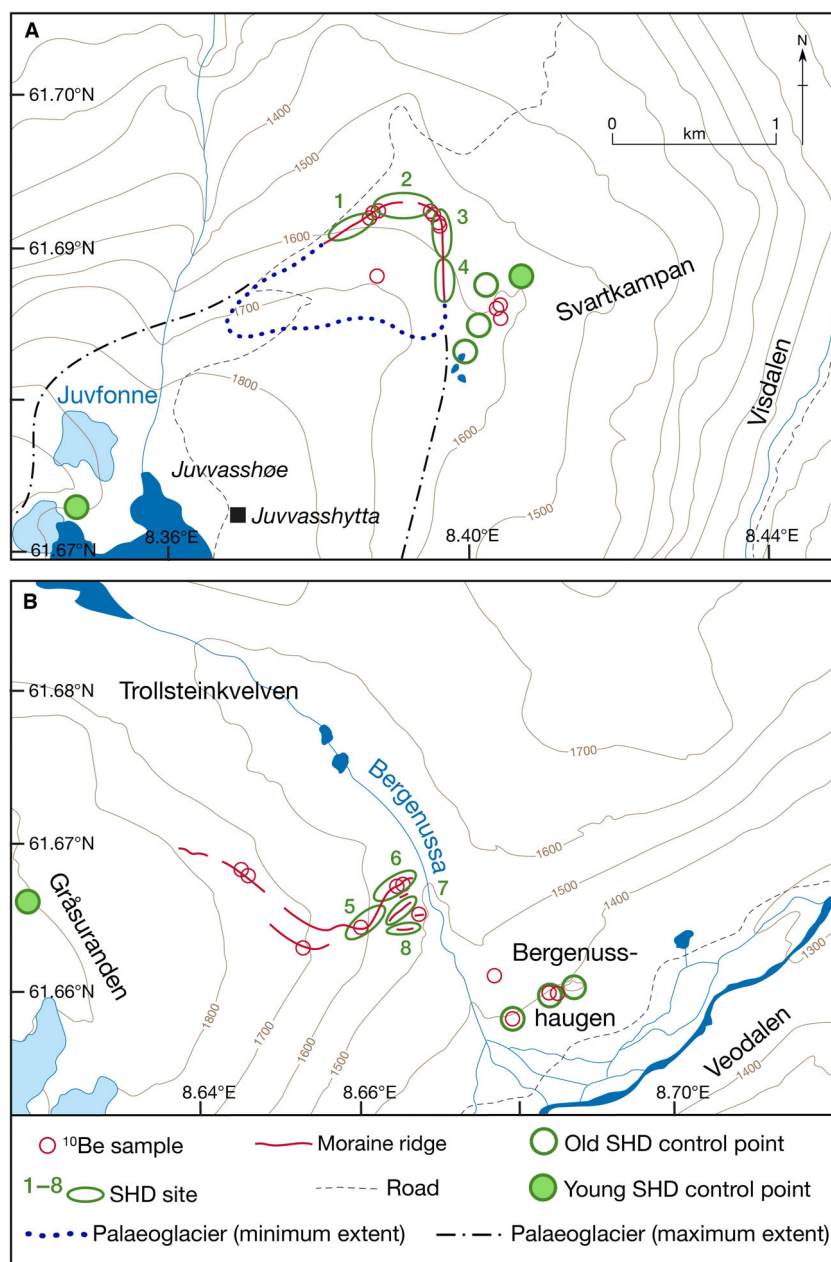
*Fig. 3.* Maps of the Galdhøpiggen (A) and Glittertinden (B) study areas at the same scale (indicated in A) showing the location of moraines ridges (thick red lines), boulder and bedrock samples for [10]Be dating (small red circles; see Table 1 for precise coordinates), areas of moraine boulders sampled for SHD (numbered green ovals) and control points for SHD (large green circles). The site of the young control point for SHD in the Glittertinden area is on the glacier foreland of Gråsubrean (west of Gråsuranden). Minimum and maximum extent of the palaeoglacier at the Galdhøpiggen site are also shown. Additional details on the landscape settings of the moraines are available from topographic maps and aerial images in Figs S1 and S2.

(1397–1476 m a.s.l.) significantly below the elevation of the moraine belt. The purpose of the latter four samples was to test further the age of the moraine ridges and constrain the timing of the subsequent retreat of the palaeoglacier from the moraine belt. In addition, we wanted to check the bedrock for nuclide inheritance, despite frequent observations of striations, glacial polish and grooves. This was also the purpose of collecting a

single bedrock sample from a quartz vein in syenitic gneiss on Søre Brurskardsknappen, about 26 km south of the Glittertinden sites, but proximal to the ~11 cal. ka BP lake site of Velle *et al.* (2010).

A total of 23 rock samples (Fig. S4) were collected from the top surfaces of boulders and bedrock outcrops using a hammer and chisel. To minimize the effect of post-depositional landform degradation, samples were

preferably taken from large and (sub-)horizontal boulder surfaces of suitable composition (Table S2). Sample locations were recorded using a handheld GPS (Garmin Montana 600) and checked against the digital terrain model of the area. Elevations from the digital terrain model are used when calculating site-specific [10]Be production rates. Topographic shielding at each sampling location is based on clinometer readings to the skyline at 20 (JUV samples) and 15 (BER, BRU samples) degrees azimuth intervals, and calculated according to Dunne *et al.* (1999). Field and laboratory information used for calculating surface exposure ages are given in Table 1.

Sample processing took place in the Preparation Facility for Cosmogenic Nuclides at the University of Bergen (Data S1, Table S3). Beryllium isotope ratios were measured at the Aarhus AMS Centre, Aarhus University, Denmark (Data S2).

The erosion rate used (1.5 mm ka[−1]) is based on assessing the surface relief for each sampled surface (Table S2), and by measuring the surface relief from additional 12 surfaces with protruding quartz veins and lenses (Fig. S5) in the vicinity of samples JUV 1909–1911. Quartz veins and lenses typically protrude 15–20 mm above the rock surface. This is consistent with field observations of protruding quartz veins on bedrock outcrops previously scoured by glaciers in Jotunheimen (Matthews & Owen 2011) and elsewhere in the Scandinavian mountains (André 2002; Owen *et al.* 2007; Nicholson 2009; Linge *et al.* 2020). Based on the abovementioned observations, the extreme range of erosion rates from crystalline lithologies at Scandinavian sites appears to be from 0.2 to 4.8 mm ka[−1]. The highest rates are, however, atypical for the well-drained surfaces of both bedrock outcrops and the boulders associated with exposed moraine crests. The chosen erosion rate amounts to a correction of about 120 years for an exposure period of 10 ka. An erosion rate of 1.0 mm ka[−1] would lead to a correction of about 80 years, whereas a higher rate of 2.0 mm ka[−1] would give a correction of about 165 years. The correction for erosion is thus less than half of the typical analytical uncertainty in the dataset.

Snow shielding was estimated from the modelled mean annual snow thickness and snow-cover duration for two locations for the JUV samples (1564 and 1661 m a.s.l.) and one location for the BER samples (1645 m a.s.l.), assuming a snow density of 0.3 g cm^{−3} and an attenuation length of 160 g cm^{−3} (cf. Vermeesch 2007). Snow density measured at Juvfonne in May 2020 was 0.4 g cm^{−3} (Kjøllmoen *et al.* 2021). Using one-quarter of the present-day snow thickness (Table S1) is a tentative value based on the difference between uplift-corrected [10]Be ages from mid -to high-elevation Younger Dryas sites and their inferred or independently dated early/late Younger Dryas age (Data S3). It seems to accommodate wind effects (thinner snow cover) on positive landforms,

as well as reduced thickness and duration of snow cover at lower elevations and during the Holocene Thermal Maximum. No boulder-height correction was applied to the snow thickness data (cf. Heyman *et al.* 2016) as our boulders are relatively small.

After performing preliminary estimates of surface exposure ages, where topographic shielding, rock surface erosion and snow shielding were considered, an evaluation of the site's uplift history was made. We have applied a simplified approach to glacio-isostatic rebound (land uplift). Juvvasshøe is located approximately on the same isobase as Verdalsøra (Lyså *et al.* 2008; Vorren *et al.* 2008), i.e. these locations have similar relative sea-level changes since the termination of the last glaciation at the end of the Younger Dryas (~12 ka). We use the shape of the relative sea-level curve from Verdalsøra to estimate the elevation changes in 500-year increments at Juvvasshøe and Bergenussa. Approximately 70% of the elevation change occurred before 8 ka and the remainder thereafter. The relative uplift at Juvvasshøe was calculated by extrapolating the isobases along the Sognefjord to Jotunheimen, which yields a total uplift of 194 m since 12 ka. At Juvvasshøe, a 12-ka surface has a mean elevation 56 m (3.6%) lower than today, a 11-ka surface 45 m (2.9%) lower than today, and a 10-ka surface 36 m (2.3%) lower than today. We use 11.5 ka as the total exposure duration, regardless of the ages obtained from individual boulder surfaces. The mean elevation for the last 11.5 ka is 50 m lower than the present-day elevation at Juvvasshøe and 53 m lower at Veodalen. Our simplified approach differs from the ICE-6G (Peltier *et al.* 2015) based 'Correct for Elevation Change' tool available from iceTEA (http://ice-tea. org) output in two aspects: (i) a quantifiable uplift uncertainty is not included, leading to an underestimation of the age uncertainties; and (ii) the palaeo-elevation at the time of landform formation is used, instead of the apparent onset of exposure based on nuclide concentrations.

All [10]Be ages are calculated using version 3 of the online exposure age calculator (https://hess.ess. washington.edu; Balco *et al.* 2008). We use the global [10]Be production rate (Borchers *et al.* 2016), and the LSDn scaling scheme (Lifton *et al.* 2014). Both the western Norway and Scandinavian production rates yield higher ages than the global production rate, ~1.3% and 4.5%, respectively (Table S4), but our choice is based on an assessment of the consistency of dating results for suites of YD landforms using different production rates (global, western Norway, Scandinavian) and scaling models (Lm, LSDn). This exercise showed that the Scandinavian production rate overestimates YD ages when correcting for glacial isostatic uplift. The western Norway production rate data set was eliminated from consideration because it does not contain high-elevation surfaces, leaving only a global production rate. The

*Table 1.* Field and laboratory data, and $^{10}$Be surface exposure ages from Galdhøpiggen and Glittertinden in Jotunheimen. Error-weighted mean $^{10}$Be ages exclude *-labelled values, following chi-squared analysis from applying the 'Same landform' tool in version 3 of the online calculator (Balco *et al.* 2008; https://hess.ess.washington.edu).

| Sample ID | Latitude (°N) | Longitude (°E) | Elevation (m a.s.l.) | Thickness (cm) | Topographic shielding | Quartz (g) | Be spike (µg) | $^{10}$Be/$^9$Be (×10$^{-15}$)[1] | $^{10}$Be concentration (10$^4$ at g$^{-1}$ SiO$_2$)[1] | $^{10}$Be surface exposure age (ka)[2] ±internal (external) uncertainty | |
|---|---|---|---|---|---|---|---|---|---|---|---|
| | | | | | | | | | | Estimated age[3] | Corrected age[4] |
| *Galdhøpiggen–Juvvasshoe, erratic boulders* | | | | | | | | | | | |
| JUV 1901 | 61.688174 | 8.403171 | 1611 | 1.5 | 0.9998 | 19.99949 | 287±1 | 212.7±7.0 | 18.0±0.6 | 10.48±0.36 (0.72) | 11.31±0.40 (0.79) |
| JUV 1902 | 61.687756 | 8.401932 | 1612 | 3.0 | 0.9995 | 20.07821 | 286±1 | 214.6±10.7 | 18.1±0.9 | 10.64±0.55 (0.84) | 11.49±0.60 (0.92) |
| JUV 1903 | 61.686346 | 8.397707 | 1636 | 2.5 | 0.9995 | 19.82322 | 287±1 | 204.9±7.8 | 17.5±0.7 | 10.04±0.40 (0.72) | 10.82±0.44 (0.78) |
| | | | | | | | | | Mean age±SD | 10.39±0.31 | 11.21±0.34 |
| | | | | | | | | | Error-weighted mean age±int (ext) | 10.35±0.24 (0.66) | 11.16±0.26 (0.72) |
| *Galdhøpiggen–Juvvasshoe, moraine boulders east* | | | | | | | | | | | |
| JUV 1905 | 61.694144 | 8.390919 | 1561 | 1.0 | 0.9995 | 20.03271 | 286±1 | 206.0±6.5 | 17.4±0.6 | 10.49±0.34 (0.71) | 11.33±0.38 (0.78) |
| JUV 1906 | 61.694251 | 8.390842 | 1561 | 3.0 | 0.9991 | 20.00426 | 286±1 | 201.5±6.9 | 17.0±0.6 | 10.43±0.37 (0.72) | 11.26±0.41 (0.79) |
| JUV 1907* | 61.694421 | 8.390687 | 1559 | 1.0 | 0.9991 | 20.94069 | 286±1 | 280.7±9.0 | 22.7±0.7 | 13.80±0.45 (0.93) | 14.93±0.50 (1.03) |
| JUV 1908* | 61.694555 | 8.390477 | 1557 | 3.0 | 0.9991 | 20.09172 | 286±1 | 117.0±5.0 | 9.8±0.4 | 5.98±0.27 (0.45) | 6.41±0.29 (0.48) |
| | | | | | | | | | Mean age±SD | 10.18±3.21 | 10.98±3.50 |
| | | | | | | | | | Error-weighted mean age±int (ext) | 10.46±0.25 (0.67) | 11.30±0.28 (0.73) |
| *Galdhøpiggen–Juvvasshoe, moraine boulders west* | | | | | | | | | | | |
| JUV 1909* | 61.694287 | 8.384830 | 1566 | 1.0 | 0.9989 | 19.99906 | 286±1 | 250.1±8.1 | 21.1±0.7 | 12.78±0.43 (0.87) | 13.81±0.47 (0.96) |
| JUV 1910 | 61.694260 | 8.384811 | 1566 | 1.5 | 0.9989 | 20.33151 | 286±1 | 215.5±8.0 | 17.9±0.7 | 10.83±0.42 (0.76) | 11.68±0.46 (0.84) |
| JUV 1911 | 61.694396 | 8.385054 | 1564 | 2.5 | 0.9989 | 19.94146 | 286±1 | 217.5±7.7 | 18.4±0.7 | 11.25±0.41 (0.78) | 12.15±0.45 (0.86) |
| | | | | | | | | | Mean age±SD | 11.62±1.03 | 12.55±1.12 |
| | | | | | | | | | Error-weighted mean age**±int (ext) | 11.04±0.30 (0.72) | 11.92±0.32 (0.78) |
| *Galdhøpiggen–Juvvasshoe, all moraine boulders* | | | | | | | | | | | |
| | | | | | | | | | Mean age±SD | 10.79±2.47 | 11.65±2.69 |
| | | | | | | | | | Error-weighted mean age**±int (ext) | 10.71±0.19 (0.66) | 11.56±0.21 (0.73) |
| *Galdhøpiggen–Juvvasshoe, bedrock* | | | | | | | | | | | |
| JUV 2201 | 61.689068 | 8.386181 | 1694 | 1.5 | 0.9958 | 20.16967 | 255±1 | 188.0±7.0 | 15.8±0.6 | 7.76±0.29 (0.54) | 8.32±0.32 (0.59) |
| *Glittertinden–Bergenussa west, all moraine boulders* | | | | | | | | | | | |
| BER 2101 | 61.664373 | 8.652575 | 1718 | 1.0 | 0.9994 | 20.06438 | 256±1 | 253.5±6.4 | 21.7±0.5 | 10.36±0.26 (0.67) | 11.20±0.29 (0.73) |
| BER 2102* | 61.669547 | 8.643091 | 1759 | 1.0 | 0.9996 | 20.03534 | 256±1 | 220.3±6.8 | 18.8±0.6 | 8.70±0.27 (0.58) | 9.38±0.29 (0.63) |
| BER 2103* | 61.66935 | 8.643585 | 1757 | 1.5 | 0.9996 | 20.09886 | 256±1 | 199.6±4.9 | 17.0±0.4 | 7.89±0.20 (0.51) | 8.48±0.21 (0.55) |
| BER 2104 | 61.666446 | 8.659426 | 1621 | 2.0 | 0.9983 | 20.30289 | 256±1 | 236.8±5.3 | 20.0±0.5 | 10.43±0.24 (0.66) | 11.29±0.26 (0.73) |
| BER 2201 | 61.669759 | 8.663186 | 1570 | 1.0 | 0.9994 | 20.18160 | 255±1 | 235.9±9.7 | 19.9±0.8 | 10.74±0.45 (0.78) | 11.62±0.49 (0.85) |
| BER 2202 | 61.669687 | 8.662998 | 1571 | 1.5 | 0.9994 | 20.33932 | 255±1 | 223.0±7.0 | 18.7±0.6 | 10.10±0.33 (0.69) | 10.93±0.35 (0.74) |
| BER 2203* | 61.667917 | 8.666304 | 1528 | 3.5 | 0.9987 | 20.41903 | 255±1 | 264.0±6.9 | 22.0±0.6 | 12.75±0.34 (0.82) | 13.63±0.37 (0.90) |
| | | | | | | | | | Mean age±SD | 10.11±1.51 | 10.93±1.65 |
| | | | | | | | | | Error-weighted mean age**±int (ext) | 10.38±0.15 (0.63) | 11.22±0.16 (0.69) |
| *Glittertinden–Bergenusshaugen, erratic boulders on bedrock* | | | | | | | | | | | |
| BER 2105 | 61.664105 | 8.678658 | 1476 | 1.5 | 0.9995 | 20.15302 | 256±1 | 211.2±5.3 | 17.9±0.5 | 10.50±0.27 (0.68) | 11.38±0.30 (0.74) |
| BER 2204 | 61.661153 | 8.683333 | 1364 | 2.0 | 0.9950 | 20.17498 | 255±1 | 184.4±7.0 | 15.5±0.6 | 10.07±0.39 (0.71) | 10.91±0.43 (0.78) |
| | | | | | | | | | Mean age±SD | 10.29±0.31 | 11.14±0.33 |
| | | | | | | | | | Error-weighted mean age±int (ext) | 10.36±0.22 (0.65) | 11.22±0.24 (0.72) |
| *Glittertinden–Bergenusshaugen, bedrock* | | | | | | | | | | | |
| BER 2205 | 61.663635 | 8.688879 | 1404 | 2.0 | 0.9980 | 20.43361 | 255±1 | 207.9±6.2 | 17.3±0.5 | 10.83±0.33 (0.72) | 11.72±0.36 (0.79) |

(continued)

*Table 1.* (continued)

| Sample ID | Latitude (°N) | Longitude (°E) | Elevation (m a.s.l.) | Thickness (cm) | Topographic shielding | Quartz (g) | Be spike (µg) | $^{10}Be/^{9}Be$ ($\times 10^{-15}$)[1] | $^{10}Be$ concentration ($10^4$ at g$^{-1}$ SiO$_2$)[1] | $^{10}Be$ surface exposure age (ka)[2] ±internal (external) uncertainty Estimated age[3] | Corrected age[4] |
|---|---|---|---|---|---|---|---|---|---|---|---|
| BER 2206 | 61.663521 | 8.686387 | 1397 | 1.0 | 0.9919 | 20.29669 | 255±1 | 184.3±6.5 | 15.4±0.5 | 9.68±0.35 (0.67) | 10.46±0.38 (0.73) |
| | | | | | | | | | Mean age±SD | 10.25±0.81 | 11.09±0.89 |
| | | | | | | | | | Mean age±int (ext) | 10.25±0.81 (1.02) | 11.09±0.89 (1.11) |
| *Søre Brurskardsknappen, bedrock*[5] | | | | | | | | | | | |
| BRU 2201 | 61.442059 | 8.82199 | 1404 | 1.5 | 0.9991 | 19.89639 | 255±1 | 360.3±13.6 | 30.8±1.2 | 19.22±0.73 (1.36) | 20.55±0.79 (1.45) |

[1]All AMS targets were prepared at the UiB Cosmogenic Nuclide Preparation Facility and measured at Aarhus AMS Centre. $^{10}Be/^{9}Be$ isotope ratios are normalized to the ICN-01-5-4 Be standard assuming a $^{10}Be/^{9}Be$ nominal value of $2.851 \times 10^{-12}$ (Nishiizumi *et al.* 2007). One chemistry $^{10}Be/^{9}Be$ blank (UiB 1908) with a ratio of ($6.199\pm1.053$) $\times 10^{-15}$ is included in the JUV 19 sample batch. One chemistry $^{10}Be/^{9}Be$ blank (UiB 2107) with a ratio of ($0.479\pm0.364$) $\times 10^{-15}$ is included in the BER 21 sample batch. One chemistry $^{10}Be/^{9}Be$ blank (UiB 2205) with a ratio of ($0.537\pm0.369$) $\times 10^{-15}$ is included in the JUV-BER-BRU 22 sample batch. The reported $^{10}Be$ concentrations are the blank corrected values. Uncertainties include error of the blank and counting statistics.

[2]Surface exposure ages are calculated using 'The online exposure age calculator formerly known as the CRONUS-Earth online exposure age calculator' (Balco *et al.* 2008) using a density value of 2.65 g cm$^{-1}$ for all samples, the global $^{10}Be$ production rate (CRONUS-Earth Primary of Borchers *et al.* 2016) and LSDn scaling (Lifton *et al.* 2014). Internal uncertainties are measurement uncertainties, external uncertainties (in parentheses) include uncertainty of the $^{10}Be$ production rate and the $^{10}Be$ decay constant. The 'single landform' tool of the calculator provides Mean ages (±SD) and error-weighted mean ages (±internal uncertainty (external uncertainty)). \*\*Error-weighted mean ages exclude outliers (marked with \*).

[3]'Raw' ages have been calculated as described above ([2]) with site-specific topographic shielding, no atmospheric change, and no inheritance.

[4]'Corrected' ages have been calculated as described above ([2]) with site-specific topographic shielding, assuming erosion rates of 1.5 mm ka$^{-1}$, 25% of the modelled modern (AD 1958–2020) snow shielding, i.e. 2.0% lower nuclide production, a glacio-isostatic rebound correction since 11.5 ka (50 m lower mean elevation for JUV surfaces, 53 m for BER surfaces, 56 m for BRU surface) and no inheritance.

[5]Results from complementary Al AMS analysis at Aarhus AMS Centre: $^{26}Al/^{27}Al$ isotope ratio is normalized to the ICN-01-5-2 Al standard ($1.82 \times 10^{-12}\pm1.1\%$ ($1\sigma$); Nishiizumi 2004). One chemistry $^{26}Al/^{27}Al$ blank (UiB 2205) with a ratio of ($1.07\pm0.330$) $\times 10^{-14}$ is included in the JUV-BER-BRU 22 sample batch. The blank corrected $^{26}Al$ concentration for BRU 2201 is ($19.67\pm5.12$) $\times 10^4$. Uncertainties are reported at the 1$\sigma$ confidence level, and the propagated uncertainties include error of the blank and counting statistics. The $^{26}Al/^{10}Be$ ratio is 6.4±0.3, indicating a complex surface exposure history for the sampled surface.

rationale behind our choice of production rate and scaling model is further elaborated in Data S3, S4 and Table S4.

Table 1 shows both estimated 'raw' ages (Fig. S6) and corrected ages. The corrections include erosion (1.5 mm ka$^{-1}$), one-quarter of the modern snow shielding (2%) and glacio-isostatic uplift (average elevation since 11.5 ka). Erosion and snow shielding lead to ~3.5% higher ages, which increases to ~8% when uplift is included. Only the corrected ages are used throughout this paper as they are the closest approximations to the true ages of the moraines. In order of decreasing impact, the main uncertainties are associated with the quantification of snow shielding, the precision of the uplift history and the representativeness of the erosion rate, for the entire exposure period.

*Sampling and analysis for SHD*

Using a mechanical N-type Schmidt hammer (Proceq 2017), large samples of *R*-values (rebound values) were collected from boulders on moraine ridges and glacially scoured bedrock outcrops. Sampling was designed to produce SHD age determinations that are both complementary and directly comparable with the [10]Be ages. At each of four Galdhøpiggen moraine-ridge sites (Fig. 3A), sample sizes of 200 *R*-values were obtained and a single impact was taken from each boulder. Four sites were also sampled from the Glittertinden moraine belt, again using sample sizes of 200 impacts: two from the outer ridge, one from the inner ridge and one from an intermediate ridge (Fig. 3B). Similar sample sizes (*n* = 200) were used at 'inside' sites in the Glittertinden area (three bedrock sites and two associated sites involving erratic boulders perched on these bedrock outcrops, all located at elevations below the moraine belt). Sample sizes from additional rock surfaces used for age calibration in the Galdhøpiggen area are described below.

On the basis of a large number of SHD applications to gneissic rock surfaces in southern Norway, sample sizes of at least 200 *R*-values are sufficient to ensure an age resolution of <1000 years (Matthews & Winkler 2022). *R*-Value distributions from the moraine ridges (Fig. 4) show symmetrical distributions with little or no evidence of departure from normality (see also the skewness and kurtosis values in Table 3) or multimodality that might indicate boulder populations of mixed age (Matthews & Winkler 2022). Combining the data from adjacent sites was expected to produce an age resolution of ~500 years or less, while subsamples of 100 impacts permitted the inspection of within-site *R*-value variability and the detection of possible post-depositional disturbance effects. As boulders were sufficiently abundant, the use of one impact per boulder was favoured in order to take between-boulder *R*-value variability fully into account. Clusters of impacts were taken from several different

parts of each of the bedrock outcrops to account for within-outcrop *R*-value variability.

Lithological, micro-topographical and other micro-environmental differences between boulder and bedrock surfaces were eliminated as much as possible during sampling. Although lithological inhomogeneity could not be completely eliminated, boulder and bedrock surfaces of the dominant regional pyroxene–granulite gneiss were impacted and less common lithologies were avoided. Following common principles and practice in previous applications (e.g. Sumner & Nel 2002; Shakesby *et al.* 2006; Aydin 2009; Matthews & Owen 2010; Karakul 2017, 2020), impacts were confined to horizontal or subhorizontal rock surfaces at points with an absence of lichen cover. Structural defects, cracks, edges and wet or moist rock surfaces were avoided and only stable boulders that did not move when impacted were used. The requirement of a minimum boulder size or weight did not therefore arise (cf. Goudie 2006; Stahl *et al.* 2013; Winkler *et al.* 2016, 2020). Focusing of sampling on upstanding outcrops and the crests of moraine ridges at locations within a relatively narrow elevation range went a considerable way towards holding constant any microclimatic effects (particularly those affected by snow depth and duration) on weathering rates and hence *R*-values.

No abrasive pretreatment of the rock surfaces was attempted prior to Schmidt hammer measurement on the grounds that artificial abrasion is likely to remove weathering as well as non-weathering roughness effects and therefore to be counterproductive in the context of SHD (see discussion in Matthews & Winkler 2022). Similarly, apart from the rejection of particular anomalous *R*-values for specific reasons for which there was evidence (such as slippage of the instrument during measurement or the presence of structural flaws at the point of impact), no systematic rejection of high- or low-value outliers was deemed necessary or beneficial.

Age calibration was carried out separately for the Galdhøpiggen and Glittertinden areas. It involved establishing linear numerical relationships (calibration equations) between *R*-value and rock-surface age using two (young and old) control surfaces of known age. This 'two-point' solution to age calibration was first proposed by Matthews & Owen (2010), and has since been widely applied (see Matthews & Winkler 2022). In this paper we have used several sites on boulders and/or bedrock, which have been weighted equally and combined to establish each control point. Despite an underlying non-linear (negative exponential) rate of chemical weathering of rock surfaces over longer timescales (Colman 1981; Colman & Dethier 1986; Tomkins *et al.* 2018b), the relationship between *R*-value and surface age, particularly of resistant lithologies, has been shown to be approximately linear over the shorter timescale of the Holocene and Lateglacial (Shakesby *et al.* 2011; Tomkins *et al.* 2016, 2018a; Matthews & Winkler 2022). The
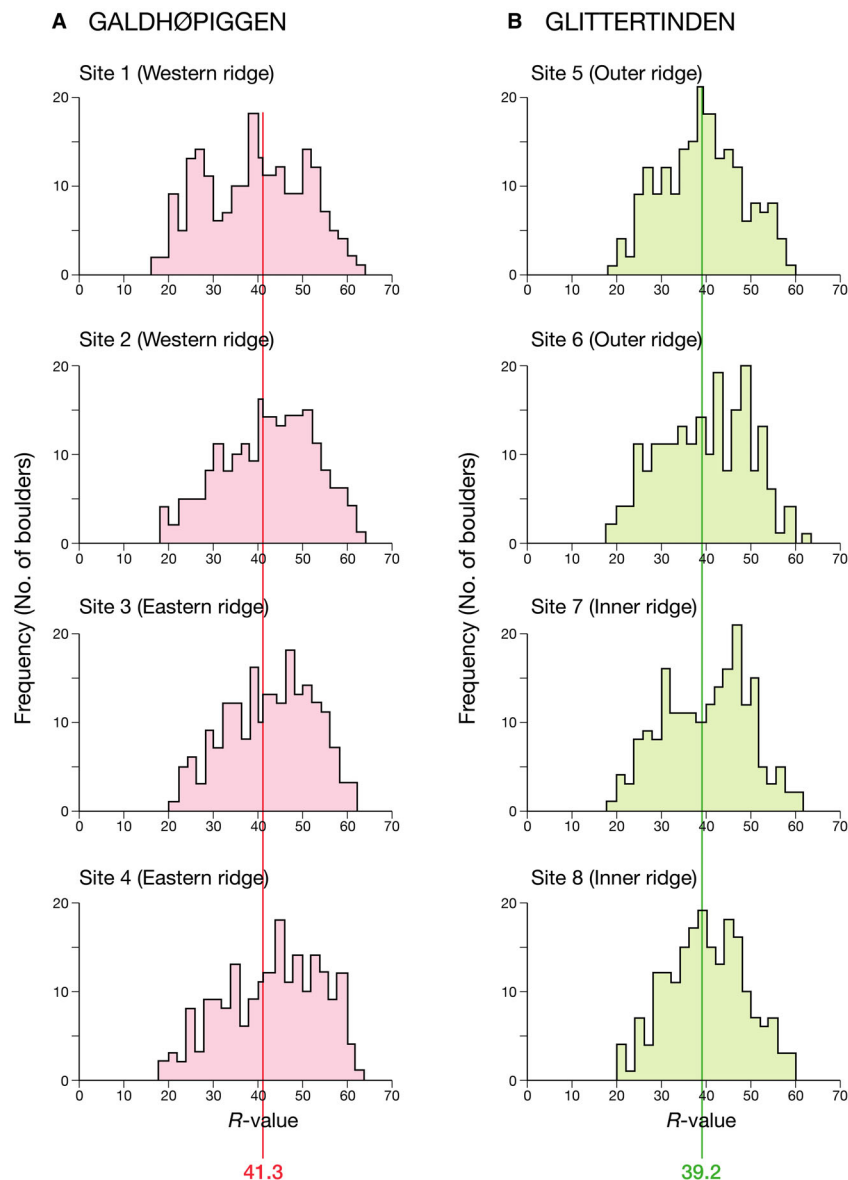
*Fig. 4.* *R*-Value frequency histograms for moraine-ridge sites in the (A) Galdhøpiggen (red) and (B) Glittertinden (green) areas. Vertical lines indicate overall mean *R*-values for the four sites in each area (see Table 3 for numerical values of skewness and kurtosis).

approach is therefore justifiable, provided the control-point ages used for SHD are independent of the *in situ* cosmogenic nuclide ages used to date the moraine ridges.

Putting the full approach into practice involves a series of nine equations, which have been summarized most recently in Matthews & Winkler (2022). Each SHD age is predicted with a 95% confidence interval (*Ct*) produced by combining the 95% confidence interval of the calibration equation (*Cc*; the calibration error) with the 95% confidence interval associated with the surface being dated (*Cs*; the sampling error). Both *Cc* and *Cs* depend on *R*-value variability and sample size. The method makes at least three assumptions: (i) the calibration equation is indeed linear; (ii) the control

points and the surfaces to be dated have identical lithologies; and (iii) the ages assigned to the control points are accurate. The 'two-point' solution to age calibration was necessary as additional surfaces of known age are not available from the study area. It should also be noted that several studies utilizing multiple control points spread over the entire Holocene on comparable lithologies (e.g. Shakesby *et al.* 2011) confirm that a linear SHD-calibration equation is a suitable selection for our time scale.

To allow an independent dating approach, the ages of the 'old' control points in this study are provided by the [10]Be ages from the erratic boulders located 'outside' the moraine in the Galdhøpiggen study area and 'inside'

the moraine belt in the Glittertinden area. *R*-values for the 'old' control point in the Galdhøpiggen area were measured previously on glacially scoured bedrock surfaces located in close proximity to the erratic boulders on Svartkampan (Fig. 3A) (Matthews *et al*. 2019). The 'young' control point in the Galdhøpiggen area utilizes *R*-values from boulders on modern deglacierized terrain at Veslejuvbreen, close to the Kjelen glacier front (Matthews *et al*. 2014), and active frost-shattered bedrock cliffs at Svartkampan (Matthews *et al*. 2019) (Fig. 3A). In the Glittertinden area, *R*-values for the 'old' control point were obtained in this study from boulders and bedrock in the immediate vicinity of the 'inside' sites dated by [10]Be while, for the 'young' control point, *R*-values from boulders measured previously on modern moraine ridges on the Gråsubrean glacier foreland (Matthews *et al*. 2014) were used (Fig. 3B).

### ELA reconstruction

The difference in the ELA between a modern glacier and a comparable palaeoglacier in the same area (ΔELA) is an index of climatic change driven by winter (accumulation season) precipitation, summer (ablation season) temperature and wind transport of (dry) snow from adjacent mountain plateaus.

Several approaches have been developed for calculating the ELAs of palaeoglaciers from their outer limits, based on the mapping of frontal and lateral moraines (e.g. Sutherland 1984; Rea 2009; Benn & Hulton 2010; Bakke & Nesje 2011; Pellitero *et al*. 2015). Here we use three relatively simple methods to estimate the ELA of the palaeoglaciers on Galdhøpiggen and Glittertinden. Previous wide use of these methods in the context of Norwegian glaciers provides necessary comparative data for interpreting our results.

- The maximum elevation of lateral moraines (MELM) simply defines the ELA as the highest elevations at which lateral moraines occur. It depends on the pattern of glacier flow, which produces lateral moraines only below the ELA where, in the ablation zone, the glacier flowlines are towards the glacier margin (Andrews 1975). The MELM underestimates the ELA if insufficient debris is available or slopes are too steep to form moraines, or if moraines have been removed by post-depositional erosion.
- The toe-to-headwall altitude ratio (THAR) locates the ELA between the maximum ($H_{max}$) and minimum ($H_{min}$) elevation of the glacier according to an empirically determined ratio (Péwé & Reger 1972; Meierding 1982). Here, we apply a ratio of 0.6, which is appropriate for steady-state glaciers. $H_{max}$ is often more difficult to define than $H_{min}$ and the THAR does not take account of glacier hypsometry or topography.
- The accumulation area ratio (AAR) takes hypsometry into account by using the ratio of the accumulation

area to the total glacier area. The AAR is commonly in the range 0.5–0.8 for steady-state glaciers (Meier & Post 1962) with significant variations associated with deviations from uniform area/elevation distributions (Nesje 1992). We follow Porter (1975), who suggested that an AAR of 0.6±0.05 is typical for valley glaciers.

All three methods were employed in the Galdhøpiggen area and corrected for land uplift (as explained above in relation to [10]Be dating). The two options considered for the outline of the palaeoglacier, estimating its minimum and maximum extent, each yielded corresponding values for the palaeo-ELA and hence ΔELA. Both options used the same position of the former glacier snout and ablation area based on the latero-terminal moraine but different positions of the headwall and accumulation area. The minimum extent of the palaeoglacier assumes an isolated ice body located beneath Juvvasshøe with a headwall at ~1740 m a.s.l. (Fig. 3A). The maximum extent of the palaeoglacier considers a much larger ice body with a headwall extending to ~2030 m a.s.l. beneath Galdhøe. Modern steady-state ELAs were based on THAR and AAR from the present outline of the Vesljuvbrean glacier (which has no lateral or terminal moraines).

In the Glittertinden area, the minimum elevation of the palaeoglacier is unknown owing to the absence of a terminal moraine, and the absence of a lateral moraine on the south side of Veodalen prevented reconstruction of the outline of the palaeoglacier. Thus, neither the THAR nor the AAR could be calculated. However, an estimate of the MELM is available from the maximum elevation attained by the moraine belt on the north side of Veodalen and the modern ELA is accurately known from mass-balance monitoring of Gråsubrean between 2010 and 2021 (http://glacier.nve.no/glacier/viewer/ci/no/). Both Gråsubrean and Vesljuvbrean are considered very appropriate topographically for estimating the modern ELA and for comparison with their respective palaeoglaciers as they are substantial glaciers that are located directly upslope of the palaeoglaciers with similar aspects.

## Results

### [10]Be ages

[10]Be surface exposure ages (LSDn scaling, global production rate), with internal and external uncertainties (±1σ) are presented in Table 1 (see also Fig. S5). When only single uncertainties are mentioned in the text, these are the internal uncertainties (appropriate for internal comparison of the dataset) unless stated otherwise. Groups of samples and within-group mean ages with excluded statistical outliers (error-weighed mean ages) are identified in Table 1. Such outliers are most likely accounted for by inheritance of

$^{10}$Be in boulders incorporated into moraines (over-estimates of moraine age) or excessive post-depositional erosion (underestimates of moraine age). Nuclide inheritance is only apparent for the BRU bedrock sample, based on the high apparent $^{10}$Be surface exposure age and an $^{26}$Al/$^{10}$Be ratio of 6.4±0.3. Raw and corrected exposure ages are also provided in Table 1 but, for reasons given above, the corrected ages are considered most realistic and are the preferred age estimates used throughout the text and in Fig. 5.

*Galdhøpiggen sites.* – The three moraine boulders from the western moraine ridge crest yielded corrected $^{10}$Be ages ranging over ~2.0 ka from 11.68±0.46 to 13.81±0.47 ka (Table 1) with a mean age of 12.55±1.12 ka. Removal of the single outlier (JUV

1909) gives an error-weighted corrected mean age of 11.92±0.32 ka. Inheritance is the most likely explanation for the anomalously old age of JUV 1909.

Four boulders from the eastern moraine ridge crest yielded corrected $^{10}$Be ages ranging from 6.41±0.29 to 14.93±0.50 ka, and a mean age of 10.98±3.50 ka. Excluding the oldest and youngest ages (both JUV 1907 and JUV 1908 are outliers), the error-weighted corrected mean age is 11.30±0.28 ka. The anomalous young age obtained for sample JUV 1908 (6.41±0.29 ka) may be the result of a slab-release event exploiting surface-parallel rock fractures. Although there is no obvious observational evidence for the anomalously old age obtained for JUV 1907 (14.93±0.50 ka), inheritance again provides a likely explanation. On the other hand, the relatively young corrected age of the single bedrock
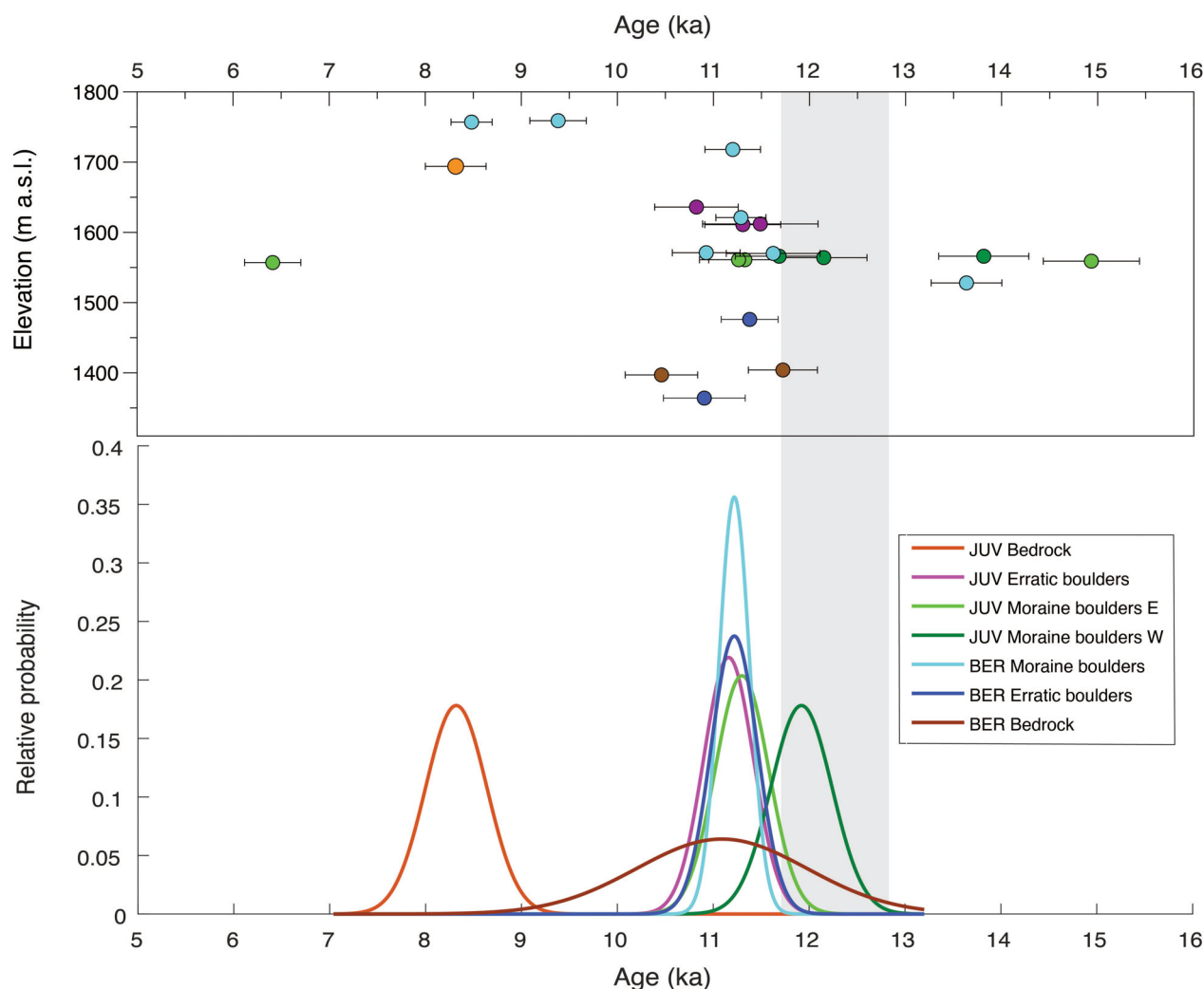


*Fig. 5.* Upper panel: individual corrected $^{10}$Be exposure ages with internal uncertainties. Lower panel: normal kernel density estimates of error-weighed maximum corrected mean $^{10}$Be exposure ages from the western and eastern moraine-ridges in the Galdhøpiggen study area (JUV Moraine boulders), the moraine belt in the Glittertinden study area (BER Moraine boulders), 'inside' sites (JUV Bedrock, BER Bedrock and BER Erratic boulders) and 'outside' sites (JUV Erratic boulders). The vertical grey band represents the Younger Dryas Stadial.

sample from inside the moraine ridge (JUV 2201; 8.32±0.32 ka) shows a lack of nuclide inheritance and indicates prolonged snow shielding as it is proximal to a modern snow field. Moreover, the bedrock exposure is located in the upper part of a modern snow field and the apparent exposure age supports prolonged snow shielding or a combination of erosion and snow shielding.

Combining all seven moraine boulders yields a corrected mean age of 11.65±2.69 ka. Removing the outliers (JUV 1907, 1908, 1909) gives an error-weighted mean corrected age of 11.56±0.21 ka (Table 1).

The erratic boulders sampled from 'outside' the limits of the proposed palaeoglacier yielded three [10]Be ages between 10.82±0.44 and 11.49±0.60 ka, all of which overlap within their analytical uncertainties (Table 1). The mean corrected age is 11.21±0.34 ka and the error-weighted mean age is 11.16±0.26 ka. Thus, the exposure age of the group of erratic boulders from the 'outside' sites cannot be distinguished from the age of the boulders on the eastern moraine ridge but appears to be ~750 years younger than the moraine boulders on the western ridge (see also Fig. 5). This small (but not statistically significant) age difference could be accounted for by environmental differences between the sites, possibly local variations in snow shielding and/or differences in weathering rate.

*Glittertinden sites.* – Three of the [10]Be ages from the Glittertinden moraine belt sites (BER 2102, 2103 and 2203) yielded outliers of 9.38±0.29, 8.48±0.21 and 13.63±0.37 ka. The young outliers may be explicable in terms of more recent/active landform degradation as this ridge segment has snow fields along both flanks. The significantly old outlier may be accounted for in terms of inheritance (Table 1). The four remaining ages

(three from the outer ridge of the moraine belt), which range from 10.93±0.35 (BER 2202) to 11.62±0.49 ka (BER 2201), are in close agreement, yielding an error-weighted corrected mean age of 11.22±0.16 ka. The age of 11.20±0.29 ka from the inner ridge (BER 2101) supports the proposition that there is no significant difference in age between the outer and inner ridges of the moraine. The [10]Be age for the Glittertinden moraine belt is therefore remarkably close to the [10]Be age of the eastern moraine ridge in the Galdhøpiggen area (i.e. 11.30±0.28 ka; see also Fig. 5).

The four age estimates of boulder and bedrock surfaces from sites 'inside' the moraine belt (BER 2105 and BER 2204, BER 2205 and BER 2206) are in excellent agreement (the range of minimum corrected ages is 10.46±0.38 to 11.72±0.36 ka). None of these 'inside' ages are anomalous, the ages of the bedrock and boulder samples do not differ significantly and their error-weighted corrected mean ages are 11.09±0.89 and 11.22±0.24 ka, respectively. Similarity in age between the moraines and the 'inside' sites points to rapid retreat of the palaeoglacier from the moraine belt once it had been constructed.

### SHD ages

Control-surface *R*-values, their known ages and the locally derived calibration equations are provided in Table 2, while *R*-values and SHD ages from the moraine ridges with their uncertainties (95% confidence intervals) are summarized in Table 3. Combined SHD ages for western and eastern parts of the single moraine ridge from the Galdhøpiggen area and the outer and inner ridges of the moraine belt from the Glittertinden area are used later for comparison with the preferred error-weighted corrected mean [10]Be ages.

*Table 2.* Control-point *R*-values, their [10]Be exposure ages (old control points) and observed modern ages (young control points) and the age-calibration equations for Galdhøpiggen and Glittertinden sites. Combined site values were used for SHD age calibration. Site code indicates lithology and type of rock surface: G = pyroxene granulite gneiss; M = mylonitized pyroxene granulite gneiss; RO = rock outcrops; Bo = boulders; SD = standard deviation; CI = 95% confidence interval; *n* = sample size (number of impacts).

| Site code | Mean | SD | CI | *n* | Mean | SD | CI | *n* | Source |
|---|---|---|---|---|---|---|---|---|---|
| | Galdhøpiggen sites ($y = 36\,413.955 - 621.712x$) | | | | | | | | |
| | Old control ([10]Be age 11.16 ka) | | | | Young control (modern age 50 years) | | | | |
| G1 (RO) | 42.42 | 9.04 | 0.94 | 355 | – | – | – | – | Matthews *et al.* (2019) |
| G2 (RO) | 38.59 | 9.16 | 0.96 | 350 | – | – | – | – | Matthews *et al.* (2019) |
| M (RO) | 41.03 | 8.57 | 0.98 | 300 | 59.66 | 5.62 | 1.12 | 100 | Matthews *et al.* (2019) |
| G3 (Bo) | – | – | – | – | 57.31 | 8.25 | 1.03 | 250 | Matthews *et al.* (2014) |
| Combined | 40.62 | 9.07 | 0.56 | 1005 | 58.49 | 6.94 | 0.73 | 350 | |
| | Glittertinden sites ($y = 31\,417.55 - 530.398x$) | | | | | | | | |
| | Old control ([10]Be age 11.22 ka) | | | | Young control (modern age 18 years) | | | | |
| G4 (RO) | 38.08 | 9.91 | 1.39 | 200 | – | – | – | – | This study |
| G5 (Bo) | 37.53 | 9.62 | 1.34 | 200 | – | – | – | – | This study |
| G6 (Bo) | 38.64 | 11.07 | 1.55 | 200 | – | – | – | – | This study |
| G7 (Bo) | – | – | – | – | 58.25 | 8.93 | 0.91 | 375 | Matthews *et al.* (2014) |
| G8 (Bo) | – | – | – | – | 60.15 | 8.46 | 0.86 | 375 | Matthews *et al.* (2014) |
| Combined | 38.08 | 10.20 | 0.82 | 600 | 59.20 | 8.70 | 0.62 | 750 | |

*Table 3.* Mean *R*-values and SHD ages for moraine-ridges from Galdhøpiggen and Glittertinden sites. SD = standard deviation; CI = 95% confidence interval; $Cs$ = sampling error of moraine ridge; $Cc$ = error component of calibration curve; $n$ = sample size (number of impacts; one impact per boulder).

| Moraine ridge | *R*-value | | | | SHD age±95% CI (ka) | $Cs$ (years) | $Cc$ (years) | $n$ |
|---|---|---|---|---|---|---|---|---|
| | Mean | SD | Skew | Kurtosis | | | | |
| *Galdhøpiggen sites* | | | | | | | | |
| Site 1 (west ridge) | 39.5 | 10.57 | 0.05 | −0.96 | 11.85±0.98 | 920 | 355 | 200 |
| Site 2 (west ridge) | 41.5 | 10.45 | −0.23 | −0.71 | 10.60±0.97 | 910 | 355 | 200 |
| Combined | 40.5 | 10.54 | −0.09 | −0.88 | 11.25±0.73 | 645 | 345 | 400 |
| Site 3 (east ridge) | 41.4 | 10.08 | −0.34 | −0.65 | 10.70±0.95 | 875 | 355 | 200 |
| Site 4 (east ridge) | 42.8 | 10.67 | −0.28 | −0.82 | 9.80±1.00 | 925 | 360 | 200 |
| Combined | 42.1 | 10.39 | −0.29 | −0.73 | 10.25±0.73 | 640 | 355 | 400 |
| *Glittertinden sites* | | | | | | | | |
| Site 5 (outer ridge) | 38.5 | 9.10 | 0.02 | −0.70 | 11.00±0.80 | 675 | 435 | 200 |
| Site 6 (outer ridge) | 39.3 | 9.97 | −0.09 | −0.95 | 10.55±0.85 | 735 | 430 | 200 |
| Combined | 38.9 | 9.54 | −0.03 | −0.84 | 10.80±0.45 | 500 | 430 | 400 |
| Site 7 (inner ridge) | 39.6 | 9.51 | −0.14 | −0.78 | 10.40±0.82 | 705 | 425 | 200 |
| Site 8 (inner ridge) | 39.5 | 8.56 | 0.03 | −0.61 | 10.45±0.75 | 635 | 430 | 200 |
| Combined | 39.5 | 9.08 | −0.08 | −0.68 | 10.45±0.45 | 445 | 420 | 400 |

*Galdhøpiggen sites.* – The SHD age estimates from Galdhøpiggen moraine-ridge sites (1–4) range over ~2.0 ka from 9.80±1.00 to 11.85±0.98 ka. Confidence intervals of approximately 1.0 ka indicate that the age differences between these two extremes of the range are statistically significant. However, the differences between the age estimates from within each part of the ridge are not statistically significant: those from the western part (sites 1 and 2) differ by 1.25 ka whereas those from the eastern part (sites 3 and 4) differ by 0.90 ka. In the absence of clear outliers, therefore, it is justifiable to combine the SHD results for each pair of sites, yielding combined SHD ages of 11.25±0.73 and 10.25±0.73 ka, respectively, for the western and eastern parts of the ridge. As the difference between these combined ages of 1.0 ka is not statistically significant, it is a reasonable conclusion that the two parts of the ridge are of similar age. Variability in age may nevertheless be affected by differences in weathering rate between sites caused by such factors as minor lithological variation, moisture availability and/or snow distribution: higher rates would correspond with relatively low *R*-values and hence yield relatively old ages.

*Glittertinden sites.* – The four SHD age estimates from the Glittertinden moraine belt (sites 5–8) range from 10.40±0.82 to 11.00±0.80 ka (Table 3), a difference of 0.6 ka. As the confidence intervals of the individual age estimates lie between 0.75 and 0.85 ka (a little less than those for the Galdhøpiggen moraine), none of the four age estimates differ statistically from each other. The combined ages from the outer and inner moraine ridges of 10.80±0.45 and 10.45±0.45 ka, respectively, are also more consistent than the results from the single Galdhøpiggen moraine ridge (the two Glittertinden combined ages differ by only 0.35 ka). Consistent ages indicate that the ridges within the Glittertinden moraine

belt are all of closely similar age and also that between-site lithological and/or environmental differences within the moraine belt are likely to be less than those associated with the Galdhøpiggen moraine ridge.

### *ΔELA*

The modern glacier ELA estimates for the Glittertinden area using the THAR and AAR methods are 2025 and 2050 m a.s.l., respectively (Table 4). These estimates are close to and therefore corroborated by modern mass-balance monitoring at Gråsubrean, which indicates a

*Table 4.* Estimates of modern equilibrium-line altitude (ELA), palaeo-ELA and ΔELA in the Galdhøpiggen and Glittertinden areas using three methods: MELM = maximum elevation of lateral moraines; THAR = toe-to-headwall ratio (0.4); AAR = accumulation area ratio (0.6). Note that the glaciers have no modern lateral moraines.

| Parameter | Method | | |
|---|---|---|---|
| | MELM | THAR | AAR |
| *Galdhøpiggen area* | | | |
| Modern glacier ELA (Vesljuvbrean) | – | 1980 | 1990 |
| Palaeo-ELA (minimum glacier extent) | 1605 | 1630 | 1665 |
| Palaeo-ELA (maximum glacier extent) | 1605 | 1800 | 1825 |
| ΔELA (minimum glacier extent)[1] | −575[2] | −545 | −520 |
| ΔELA (maximum glacier extent)[1] | −575[2] | −375 | −360 |
| *Glittertinden area* | | | |
| Modern glacier ELA (Gråsubrean) | – | 2025 | 2050 |
| Palaeo-ELA | 1780 | – | – |
| ΔELA[1] | −480[3] | −440 | −465 |

[1]All ΔELA estimates include a land uplift correction of 195 m.
[2]ΔELA estimate for the Galdhøpiggen area using a modern glacier ELA of 1985 m a.s.l. (mean value of the modern ELAs estimated using the THAR and AAR methods).
[3]ΔELA estimate for the Glittertinden area using the modern steady-state ELA for Gråsubrean of 2065 m a.s.l. based on glacier mass balance-monitoring 2010–2021 (http://glacier.nve.no/glacier/viewer/ci/no/).

steady-state ELA of 2065 m a.s.l. (http://glacier.nve.
no/glacier/viewer/ci/no/). They also suggest that confi-
dence can be placed in the use of the THAR and AAR
methods in the Galdhøpiggen area, which yielded ELA
values of 1980 and 1990 m a.s.l., respectively, based on
the present outline of Vesljuvbreen. The validity of our
modern ELAs based on THAR and AAR is further
supported by the lower values (by ~45–60 m) predicted
for the Galdhøpiggen area compared with the Glittertind
area. This would be expected from the greater con-
tinentality of the latter location in eastern Jotunheimen.

The single palaeo-ELA estimate for the Glittertinden
area of 1780 m a.s.l. based on the MELM and using the
modern steady-state ELA from Gråsubrean, indicates a
ΔELA (corrected for land uplift) of −480 m (Table 4). If
this is an overestimate (which is possible owing to the
nature of the MELM), the similarity with the ΔELA
estimates using THAR and AAR of −440 and −465 m,
respectively (differing from the MELM estimate by 40 m
or less) suggests that a large overestimate is unlikely.

Minimum and maximum estimates of ΔELA for the
Galdhøpiggen area based on the MELM (using the mean
of the modern ELA estimates based on the THAR and
AAR applied to Vesljuvbreen) are both −575 m
(Table 4). This is unlikely to be a large overestimate of
the true ΔELA for the minimum palaeoglacier extent as it
lies 55 m or less from the ΔELA estimates based entirely
on the THAR or AAR. However, for the maximum
palaeoglacier extent, the THAR- and AAR-based
ΔELA estimates of −375 and −360 m, respectively, are
considerably less than the MELM-based estimate. With
no compelling reason to prefer either palaeoglacier
extent from the other, mean values of the THAR- and
AAR-based ΔELAs of −460 and −440 m are estimated
for the Galdhøpiggen area. These values are very similar
to the equivalent values estimated for the Glittertinden
area and hence an overall mean estimate of −450 m for
the ΔELA in both areas.

## Discussion

### *Exposure age of the moraines*

Comparison of the preferred ages for the moraine
ridges based on [10]Be dating and SHD (Fig. 6)
demonstrates that both exposure-age dating techniques
have insufficient age resolution to distinguish unam-
biguously between Early Holocene and Younger Dryas
ages. Including the statistical uncertainties, the range of
moraine ages lies between ~9.5 and ~12.7 ka, while
more likely age ranges based on the mean values alone
lie between ~11.2 and ~11.9 ka for [10]Be dating and
~10.3 and ~11.3 ka for SHD. However, the age
differences between the dating techniques appear to
be greater than the age differences within the moraine
sets (particularly between the western and eastern
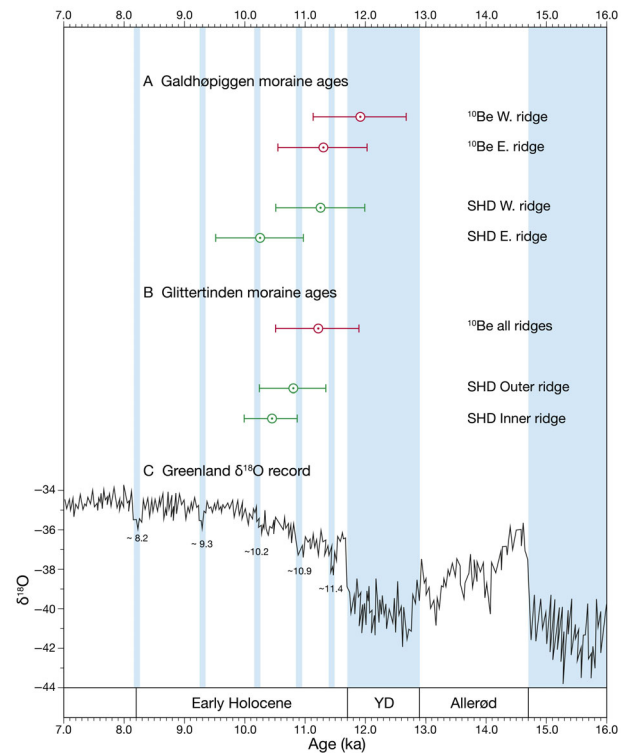Galdhøpiggen ridges). This may be accounted for by



*Fig. 6.* Graphical comparison of the preferred [10]Be and SHD ages of
the moraine ridges on (A) Galdhøpiggen and (B) Glittertinden in
relation to (C) the Greenland ice-core $\delta^{18}O$ record (after Rasmussen
*et al.* 2007, 2014). [10]Be ages (red) are error-weighted corrected mean
ages with $1\sigma$ (solid bar) external uncertainties from Table 1. SHD ages
(green) are combined mean ages (*n* = 400 impacts) with 95% confidence
intervals from Table 3. Vertical (blue) bands represent intervals of
relatively cold climate, which are recognisable in the Greenland $\delta^{18}O$
record and/or the record of southern Norwegian glacier variations.
Note the ages of five centennial-scale Early Holocene events and the
millennial-scale Younger Dryas Stadial (YD).

limitations of SHD as a calibrated-age dating technique
that assumes that the ages of the old control points are
error free as well as not being obtained from sites with
identical environmental conditions to those of the
moraine ridges. The simplest hypothesis is therefore
that both sets of moraine ridges have a similar true age
and date from either late in the Younger Dryas or very
early in the Holocene.

The true age of the moraine ridges in both the
Galdhøpiggen and Glittertinden areas is likely to
correlate with glacier advances that have been recognized
elsewhere in southern Norway and/or episodes of
relatively cold climate that have been precisely dated in
Greenland ice-core chronologies (Fig. 6C). Potential
Early Holocene events at ~8.2 and ~9.3 ka are clear in the
Greenland $\delta^{18}O$ record (Rasmussen *et al.* 2007, 2014; see
also Vinther *et al.* 2006), but can be discounted as they are
generally beyond the range of our exposure ages. Glacier
extent during the ~8.2 ka event, known as the Finse Event
in Norway (Nesje & Dahl 1991, 2001; Dahl & Nesje 1994,
1996; Nesje & Matthews 2023) was, moreover,

insufficient to account for the extent of the palaeoglaciers identified in this study. Although the ~10.2 ka event is relatively poorly defined in the Greenland ice-core chronology, it is widely recognized as associated with a glacier re-advance within the Erdalen Event in southern Norway (Nesje *et al.* 1991; Dahl *et al.* 2002; Matthews & Dresser 2008; Shakesby *et al.* 2020). Glacier extent at this time was, however, only slightly greater than during the Little Ice Age and therefore incompatible with the extent of the palaeoglaciers on Galdhøpiggen and Glittertinden (see also the discussion of ELAs below).

Our exposure-age estimates are compatible with two other Early Holocene centennial-scale events in the Greenland $\delta^{18}$O record, namely, those at ~10.9 and ~11.4 ka (Fig. 6C). The earliest Holocene event, also known as the Preboreal Oscillation (Björck *et al.* 1997; Kobashi *et al.* 2007; Mekhaldi *et al.* 2020) occurred only a few hundred years after the end of the Younger Dryas. Moraines have been attributed previously to this event in southern Norway (e.g. Fareth 1987; Bakke *et al.* 2005; Lane *et al.* 2020; Romundset *et al.* 2023) but to the authors' knowledge such moraines have not been accurately dated.

Numerous moraines, not only those delimiting the margin of the Younger Dryas ice sheet but also those deposited by mountain glaciers located beyond its western limit, have been dated to the Younger Dryas Stadial (12.9–11.7 ka) (Nesje 2009; Stroeven *et al.* 2016; Lane *et al.* 2020; Mangerud 2023; Mangerud *et al.* 2023). Based on our evidence from exposure-age dating, a Younger Dryas age is clearly possible for the moraine ridges on Galdhøpiggen and Glittertinden, but further independent evidence would be necessary to distinguish between late Younger Dryas and Early Holocene possibilities.

The error-weighted minimum-corrected mean ages of the $^{10}$Be samples from the erratic boulders located immediately 'outside' the moraine ridge in the Galdhøpiggen area (11.16±0.26 ka) and from erratic boulders (11.22±0.24 ka) and bedrock (11.09±0.89 ka) 'inside' the moraine belt in the Glittertinden area are indistinguishable both from each other and from the exposure ages from the moraine-ridges (Table 1). This strongly suggests that both the glacier advance that produced the moraines and the subsequent retreat of the glacier were part of a short-lived event during deglaciation. Otherwise, greater age differences, and hence greater time lapses would have been apparent between the moraine 'inside' and 'outside' sites.

### ELA depression of the palaeoglaciers

The ΔELA values for the Younger Dryas may have been as large as −600 to −700 m in maritime areas towards the northwestern coast of southern Norway (Larsen *et al.* 1984), and our full range of estimates for the Galdhøpiggen and Glittertinden areas is −360 to −575 m.

However, our mean estimate of −450 m for the palaeoglaciers in the Galdhøpiggen and Glittertinden areas is remarkably close to several estimates of Younger Dryas ΔELAs from the middle and inner Nordfjord area (Fareth 1987; Dahl & Nesje 1992; Nesje & Dahl 1992; Nesje 2009).

The ~ΔELA values that have been estimated for the Erdalen Event (~10.0 ka) in southern Norway are significantly lower than our estimate of −450 m from moraines deposited by the Galdhøpiggen and Glittertinden palaeoglaciers. According to Dahl *et al.* (2002), the ΔELA for the Erdalen event at Nigardsbreen did not exceed −230 m, which is close to the mean value of −270±35 m calculated by us for five outlet glaciers of the Jostedalsbreen ice cap (Erdalsbreen, Briksdalsbreen, Melkevollbreen, Bøyabreen and Nigardsbreen), lower than the mean value of −320 m for the Jostedalsbreen region as a whole (Nesje *et al.* 1991; see also Nesje & Dahl 1991; Dahl & Nesje 1992), but higher than values of −220 m from the Nordre Folgefonna ice cap (Bakke *et al.* 2005) and −205 m from the northern sector of the Hardangerjøkulen ice cap (Dahl & Nesje 1996). Although fewer values are available for the Erdalen Event in Jotunheimen, Shakesby *et al.* (2020) estimated ΔELAs of between −210 and −240 m for Styggedalsbreen, a cirque glacier in the Hurrungane massif of western Jotunheimen.

The ΔELA values from our palaeoglaciers are therefore too large to relate to the Erdalen Event and hence support our conclusion from exposure-age dating that the moraines on Galdhøpiggen and Glittertinden are older than the Erdalen Event.

Although, as noted above, moraine ridges have been attributed to the Preboreal Oscillation (~11.4 ka), Early Holocene moraines that are older than the Erdalen Event have yet to be recognized with certainty or dated accurately in southern Norway. The ΔELA values and underlying climatic fluctuations during the Preboreal Oscillation (~11.4 ka) and the ~10.9 ka event are nonetheless subject to the constraint of being intermediate in scale between those of the Erdalen Event and the Younger Dryas.

### Deglaciation at the transition from Younger Dryas to Early Holocene

Our interpretation and conceptual model of the pattern of deglaciation across the Younger Dryas–Holocene transition in the highest parts of Jotunheimen are summarized in Fig. 7A–C. This does not support traditional ice-sheet reconstructions that indicate a thick ice sheet during the Younger Dryas and early Preboreal over southern Norway, without nunataks in the Jotunheimen area (e.g. Sollid & Sørbel 1981; Sollid & Reite 1983). However, our model is consistent with a relatively thin, multidomed Younger Dryas ice sheet over central southern Norway from which we infer the
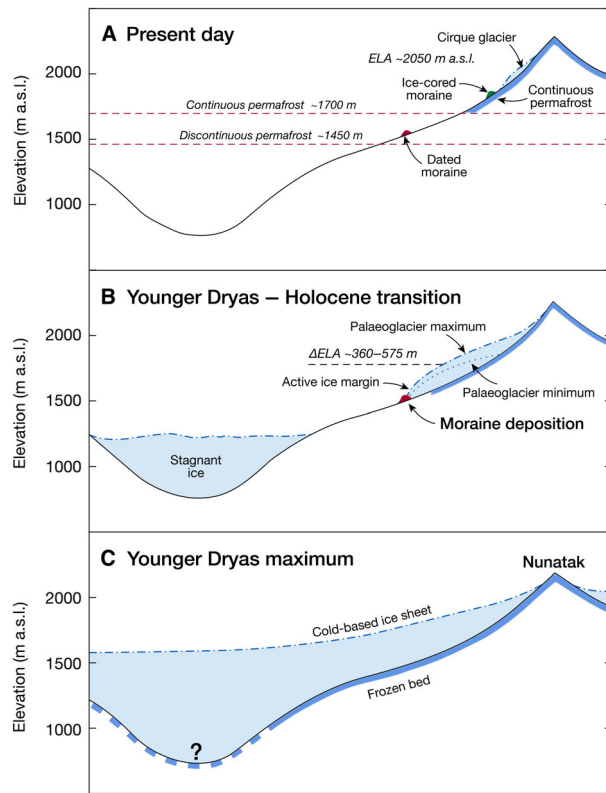
*Fig. 7.* Conceptual model of deglaciation for the highest mountains of Jotunheimen. Approximate ice extent and thickness is shown (A) at present, (B) during the Younger Dryas–Holocene transition, and (C) at the Younger Dryas maximum. In A, relict moraines (red) dated by [10]Be and SHD and Late Holocene ice-cored moraines (green) mentioned in the text are located in relation to the equilibrium-line altitude (ELA) of present-day cold-based glaciers and the present lower altitudinal limits of continuous and discontinuous permafrost. In B, the palaeoglacier (minimum and maximum extent), estimated ΔELAs, the extent of cold-based ice and continuous permafrost (dark blue), the presence of active, warm-based ice at the glacier margin and stagnant ice in an adjacent valley are shown. In C, a thin, cold-based ice sheet covers the whole landscape (apart from a nunatak with continuous permafrost) and frozen-bed conditions affect all but the areas with the thickest ice cover (indicated by '?').

presence of nunataks in Jotunheimen (cf. Dahl *et al.* 1997; Lie *et al.* 2004; Lane *et al.* 2020; Winkler *et al.* 2021; Romundset *et al.* 2023). In the absence of extensive direct dating or reliable modelling results relating to the inland areas of the ice sheet, the precise thickness of the ice sheet remains speculative.

Rapid ice wastage late in the Younger Dryas and early in the Holocene (cf. Goehring *et al.* 2008; Stroeven *et al.* 2016; Romundset *et al.* 2023) led to the isolation of most likely stagnant ice in the main valleys of Jotunheimen while on the highest mountains, individual active ice bodies continued to exist (Fig. 7B). Mapping of erosional and depositional landforms in central southern Norway (Garnes & Bergersen 1980; Sollid & Sørbel 1994) indicates that the Younger Dryas ice sheet in the Jotunheimen area was dynamically active. After

the Younger Dryas–Early Holocene transition, however, the mean annual ELA most likely rose above the ice sheet. This initiated a dynamically inactive, vertically down-wasting ice sheet with formation of lateral meltwater channels and ice dammed lakes between stagnant ice bodies in the northern parts of the valleys Gudbrands-dalen and Østerdalen and the main watershed towards Romsdalen and Trøndelag NW and north of Jotunhei-men, respectively (Romundset *et al.* 2023). In the main valleys of Jotunheimen, however, no detailed studies of potential ice-stagnation features have been carried out.

The concept of the co-existence of thin, initially still cold-based ice at high elevation with stagnant ice bodies in the main valleys and individual mountain glaciers with active margins is reminiscent of the deglaciation pattern envisaged for parts of the European Alps (Reitner *et al.* 2016; Ivy-Ochs *et al.* 2023). These active glaciers, like the present-day glaciers above ~1800 m a.s.l., probably remained in the permafrost zone (Lilleøren *et al.* 2012) and hence were cold based throughout the Holocene. In order to produce the dated moraines, however, they must have been warm based in their latero-terminal marginal zones. Thus, a short-term glacier advance led to the deposition of lateral and terminal moraines at elevations of ~1500–1800 m a.s.l. by a glacier with an equilibrium-line depression (ΔELA) of ~360–575 m (i.e. relative to the present-day ELA at 2050 m a.s.l. shown in Fig. 7A and corrected for land uplift).

According to our exposure-age dating, the advance of the palaeoglaciers that produced the dated moraines occurred either very late in the Younger Dryas or very early in the Holocene, and is likely to have occurred in response to a cold climatic fluctuation that interrupted the general trend of climatic warming at that time. Active glacier margins dated in this study may therefore represent moraine building associated with the response of the glaciers to increasing topographical control during the Younger Dryas–Early Holocene transition as the ice sheet thinned and glaciers receded into high-elevation valleys and cirques with a NE aspect (cf. Dahl *et al.* 1997; Barr & Lovell 2014). Continuing warming led to further glacier shrinkage in the later part of the Early Holocene and during the Holocene Thermal Maximum of the Middle Holocene. However, this was followed by Late Holocene cooling and neoglaciation, during which time the remaining very small cold-based glaciers were comparable in size to those surviving in the landscape today in the zone of mountain permafrost (Fig. 7A).

## Conclusions

- High-elevation moraine ridges at ~1500–1800 m a.s.l. on the Galdhøpiggen and Glittertinden massifs have mean exposure ages of ~11.6–11.2 ka ([10]Be) and ~10.8–10.6 ka (SHD).

- Allowing for the multicentury uncertainties and age resolution of both techniques, the exposure ages indicate moraine formation either towards the end of the Younger Dryas Stadial (~12.9–11.7 ka) or in the very early Holocene, associated with the Preboreal Oscillation (~11.4 ka) or the ~10.9 ka event. Formation during the Erdalen Event (~10.2–9.7 ka) can be ruled out.
- The reconstructed palaeoglaciers indicate an equilibrium-line depression (ΔELA) of ~360–575 m. Combined with the exposure ages and the morphology of the moraine ridges, this is consistent with moraine deposition during a short-lived advance of warm-based glacier margins in response to a centennial-scale (cold) climatic fluctuation.
- A conceptual model of deglaciation that takes all our results and interpretations into account supports the idea of a thin, multidomed, cold-based Younger Dryas ice sheet covering the highest mountains of southern Norway (apart from nunataks). Following ice wastage and segmentation, individual active ice bodies on the high mountains remained active and advanced during the Younger Dryas–Holocene transition while continual downwasting affected stagnant ice in the surrounding valleys.

# References

Andersen, J. L., Egholm, D. L., Knudsen, M. F., Linge, H., Jansen, J. D., Goodfellow, B. W., Pedersen, V. K., Tikhomirov, D., Olsen, J. & Fredin, O. 2019: Pleistocene evolution of a Scandinavian plateau landscape. *Journal of Geophysical Research: Earth Surface 123*, 3370–3387.

André, M. F. 2002: Rates of postglacial rock weathering on glacially scoured outcrops (Abisko-Riksgränsen area, 68° N). *Geografiska Annaler Series A (Physical Geography) 64*, 139–150.

Andreassen, L. M. (ed.) 2022: Breer og fonner i Norge. *Norges Vassdrags- og Energidirektorat (NVE), Rapport 3/2022*, 1–50.

Andreassen, L. M. & Winsvold, S. H. (eds.) 2012: Inventory of Norwegian Glaciers. *Norwegian Water Resources and Energy Directorate (NVE), Rapport 38-2012*, 242 pp.

Andrews, J. T. 1975: *Glacial Systems: An Approach to Glaciers and Their Environments.* 191 pp. Duxbury Press, North Scituate.

Aydin, A. 2009: ISRM suggested method for determination of the Schmidt hammer rebound hardness, revised version. *International Journal of Rock Mechanics and Mineral Science 46*, 627–634.

Bakke, J. & Nesje, A. 2011: Equilibrium-line altitude. *In* Singh, V. J., Singh, P. & Haritashya, U. K. (eds.): *Encyclopedia of Snow, Ice and Glaciers*, 268–277. Springer, Dordrecht.

Bakke, J., Dahl, S. O. & Nesje, A. 2005: Lateglacial and Holocene palaeoclimatic reconstruction based on glacier fluctuations and equilibrium-line altitudes at northern Folgefonna, Hardanger, western Norway. *Journal of Quaternary Science 20*, 1–20.

Balco, G. 2011: Contributions and unrealised potential contributions of cosmogenic-nuclide exposure dating to glacier chronology, 1990-2010. *Quaternary Science Reviews 30*, 3–27.

Balco, G. 2020: Glacier change and paleoclimate application of cosmogenic nuclide exposure dating. *Annual Review of Earth and Planetary Science 48*, 21–48.

Balco, G., Stone, J. O., Lifton, N. A. & Dunai, T. J. 2008: A complete and easily accessible means of calculating surface exposure ages or erosion rates from [10]Be and [26]Al measurements. *Quaternary Geochronology 3*, 174–195.

Barnett, C., Dumayne-Peaty, L. & Matthews, J. A. 2000: Holocene climatic change and tree-line response in Leirdalen, central Jotunheimen. *Review of Palaeobotany and Palynology 117*, 119–137.

Barr, I. D. & Lovell, H. 2014: A review of topographic controls on moraine distribution. *Geomorphology 226*, 44–64.

Battey, M. H. & McRitchie, W. D. 1973: A geological traverse across the pyroxene-granulites of Jotunheimen in the Norwegian Caledonides. *Norsk Geologisk Tidsskrift 53*, 237–265.

Battey, M. H. & McRitchie, W. D. 1975: The petrology of the pyroxene-granulite facies rocks of Jotunheimen, Norway. *Norwegian Journal of Geology 55*, 1–49.

Benn, D. I. & Hulton, N. R. J. 2010: An Excel™ spreadsheet program for reconstructing the surface profile of former mountain glaciers and ice caps. *Computers and Geosciences 36*, 605–610.

Björck, S., Rundgren, M., Ingólfsson, O. & Funder, S. 1997: The Preboreal oscillation around the Nordic Seas: terrestrial and lacustrine responses. *Journal of Quaternary Science 12*, 455–465.

Borchers, B., Marrero, S., Balco, G., Caffee, M., Goehring, B., Lifton, N., Nishiizumi, K., Phillips, F., Schaefer, J. & Stone, J. 2016: Geological calibration of spallation production rates in the CRONUS-Earth project. *Quaternary Geochronology 31*, 188–198.

Briner, J. P., Svendsen, J. I., Mangerud, J., Linge, H., Gyllencreutz, R., Dahl, S. O. & Fabel, D. 2023: Configuration of the Scandinavian Ice Sheet in southwestern Norway during the Younger Dryas. *Norwegian Journal of Geology 103*, 202311, https://doi.org/10.17850/njg103-3-1.

Briner, J. P., Svendsen, J. I., Mangerud, J., Lohne, Ø. S. & Young, N. E. 2014: A [10]Be chronology of south-western Scandinavian ice sheet history during the Lateglacial period. *Journal of Quaternary Science 29*, 370–380.

Colman, S. M. 1981: Rock-weathering rates as functions of time. *Quaternary Research 15*, 250–264.

Colman, S. M. & Dethier, D. P. (eds.) 1986: *Rates of Chemical Weathering of Rocks and Minerals.* 603 pp. Academic Press, Orlando.

Cook-Talbot, J. D. 1991: Sorted circles, relative-age dating and palaeoenvironmental reconstruction in an alpine periglacial environment, eastern Jotunheimen, Norway: lichenometric and weathering-based approaches. *The Holocene 1*, 128–141.

Cuzzone, J. K., Clark, P. U., Carlson, A. E., Ullman, D. J., Rinterknecht, V. R., Milne, G. A., Lunkka, J.-P., Wohlfarth, B., Marcott, S. A. & Caffee, M. 2016: Final deglaciation of the Scandinavian Ice Sheet and implications for the Holocene global sea-level budget. *Earth and Planetary Science Letters 448*, 34–41.

Dahl, S. O. & Nesje, A. 1992: Palaeoclimatic implications based on equilibrium-line altitude depressions of reconstructed Younger Dryas and Holocene cirque glaciers in inner Nordfjord, western

Norway. *Palaeogeography, Palaeoclimatology, Palaeoecology 94*, 87–97.

Dahl, S. O. & Nesje, A. 1994: Holocene glacier fluctuations at Hardangerjøkulen, central-southern Norway: a high resolution composite chronology from lacustrine and terrestrial deposits. *The Holocene 4*, 269–277.

Dahl, S. O. & Nesje, A. 1996: A new approach to calculating Holocene winter precipitation by combining glacier equilibrium-line altitudes and pine-tree limits: a case study from Hardangerjøkulen, central southern Norway. *The Holocene 6*, 381–398.

Dahl, S. O., Nesje, A., Lie, Ø., Fjordheim, K. & Matthews, J. A. 2002: Timing, equilibrium-line altitudes and climatic implications of two early Holocene glacier readvances during the Erdalen Event at Jostedalsbreen, western Norway. *The Holocene 12*, 17–25.

Dahl, S. O., Nesje, A. & Øvstedal, J. 1997: Cirque glaciers as morphological evidence of a thin Younger Dryas ice sheet in east-central southern Norway. *Boreas 26*, 161–189.

Dunne, J., Elmore, D. & Muzikar, P. 1999: Scaling factors for the rates of production of cosmogenic nuclides for geometric shielding and attenuation at depth on sloped surfaces. *Geomorphology 27*, 3–11.

Etzelmüller, B. & Hagen, J. O. 2005: Glacier-permafrost interaction in Arctic and alpine mountain environments with examples from southern Norway and Svalbard. *In* Harris, C. & Murton, J. B. (eds.): *Cryospheric Systems: Glaciers and Permafrost*, 11–27. *Geological Society, London, Special Publications 242*.

Etzelmüller, B., Berthling, I. & Sollid, J. L. 2003: Aspects and concepts on the geomorphological significance of Holocene permafrost in southern Norway. *Geomorphology 52*, 87–104.

Evans, D. J. A. 2003: Ice-marginal terrestrial land systems. *In* Evans, D. J. A. (ed.): *Glacial Landsystems*, 12–43. Arnold, London.

Farbrot, H., Hipp, T. F., Etzelmüller, B., Isaksen, K., Ødegård, R. S., Schuler, T. V. & Humlum, O. 2011: Air and ground-temperature variations observed along elevation and continentality gradients in southern Norway. *Permafrost and Periglacial Processes 22*, 343–360.

Fareth, O. W. 1987: Glacial geology of the middle and inner Nordfjord. *Norges Geologiske Undersøkelse Bulletin 408*, 1–55.

Garnes, K. & Bergersen, O. F. 1980: Wastage features of the inland ice sheet in central South Norway. *Boreas 9*, 251–269.

Goehring, B. M., Brook, E. J., Linge, H., Raisbeck, G. M. & Yiou, F. 2008: Beryllium-10 exposure ages of erratic boulders in southern Norway and implications for the history of the Fennoscandian Ice Sheet. *Quaternary Science Reviews 27*, 329–336.

Goudie, A. S. 2006: The Schmidt hammer in geomorphological research. *Progress in Physical Geography 30*, 703–718.

Gunnarsdóttir, H. 1996: Holocene vegetation history and tree-limit fluctuations in Smådalen, eastern Jotunheimen, South Norway. *Paläoklimaforschung 20*, 233–256.

Hallang, H., Froyd, C. A., Hiemstra, J. F. & Los, S. O. 2022: Tree line shifts, changing vegetation assemblages and permafrost dynamics on Galdhøpiggen (Jotunheimen, Norway) over the past ~4400 years. *The Holocene 12*, 308–320.

Hauck, C., Isaksen, K., Vonder Mühll, D. & Sollid, J. L. 2004: Geophysical surveys designed to delineate the altitudinal limit of mountain permafrost: an example from Jotunheimen, Norway. *Permafrost and Periglacial Processes 15*, 191–205.

Heyman, J., Applegate, P. J., Blomdin, R., Gribenski, N., Harbor, J. M. & Stroeven, A. P. 2016: Boulder height e exposure age relationships from a global glacial [10]Be compilation. *Quaternary Geochronology 34*, 1–11.

Hughes, A. L. C., Gyllencreutz, R., Lohne, Ø., Mangerud, J. & Svendsen, J. L. 2016: The last Eurasian ice sheets – a chronological database and time-slice reconstruction, DATED-1. *Boreas 45*, 1–45.

Isaksen, K., Hauck, C., Gudevand, E., Ødegård, R. S. & Sollid, J. L. 2002: Mountain permafrost distribution in Dovrefjell and Jotunheimen, southern Norway, based on BTS and DC resistivity tomography data. *Norwegian Journal of Geography 56*, 122–136.

Ivy-Ochs, S., Monegato, G. & Reitner, J. M. 2023: The Alps; glacial landforms during the deglaciation (18.9 - 14.6 ka). *In* Palacios, D., Hughes, P. D., García-Ruiz, J. & Andrés, N. (eds.): *European Glacial Landscapes – The Last Deglaciation*, 175–183. Elsevier, Amsterdam.

Karakul, H. 2017: Investigation of saturation effect on the relationship between compressive strength and Schmidt hammer rebound. *Bulletin of Engineering Geology and the Environment 76*, 1143–1152.

Karakul, H. 2020: Investigation of the effect of impact direction on Schmidt rebound values by multivariate regression and neuro-fuzzy models. *SN Applied Sciences 2*, 1807, https://doi.org/10.1007/s42452-020-03600-6.

Kjøllmoen, B., Andreassen, L. M., Elvehøy, H. & Melvold, K. 2021: Glaciological investigations in Norway 2020. *Norwegian Water Resources and Energy Directorate (NVE), Report 31/2021*, 95 pp.

Kleman, J. & Hättestrand, C. 1999: Frozen–bed Fennoscandian and Laurentian ice sheets during the Last Glacial Maximum. *Nature 402*, 63–66.

Kleman, J., Stroeven, A. P. & Lundqvist, J. 2008: Patterns of Quaternary ice sheet erosion and deposition in Fennoscandia and a theoretical framework for explanation. *Geomorphology 97*, 73–90.

Kobashi, T., Severinghaus, J. P. & Barnola, J.-M. 2007: 4 ± 1.5 °C abrupt warming 11,270 yr ago identified from trapped air in Greenland ice. *Earth and Planetary Science Letters 268*, 397–407.

Lane, T. P., Paasche, Ø., Kvisvik, B., Adamson, K. R., Rhodés, Á., Patton, H., Gomez, N., Gheorghiu, D., Bakke, J. & Hibbard, A. 2020: Elevation changes of the Fennoscandian Ice Sheet interior during the last deglaciation. *Geophysical Research Letters 47*, e2929GL088796, https://doi.org/10.1029/2020GL088796.

Larsen, E., Eide, F., Longva, O. & Mangerud, J. 1984: Allerød-Younger Dryas climate inferences from cirque glaciers and vegetational development in the Nordfjord area, western Norway. *Arctic and Alpine Research 16*, 137–160.

Lie, Ø., Dahl, S. O., Nesje, A., Matthews, J. A. & Sandvold, S. 2004: Holocene fluctuations of a polythermal glacier in high-alpine eastern Jotunheimen, central, southern Norway. *Quaternary Science Reviews 23*, 1925–1945.

Lifton, N., Sato, T. & Dunai, T. J. 2014: Scaling in situ cosmogenic nuclide production rates using analytical approximations to atmospheric cosmic-ray fluxes. *Earth and Planetary Science Letters 386*, 149–160.

Lilleøren, K. S. & Etzelmüller, B. 2011: A regional inventory of rock glaciers and ice-cored moraines in Norway. *Geografiska Annaler Series A (Physical Geography) 93A*, 175–191.

Lilleøren, K. S., Etzelmüller, B., Schuler, T. V., Gisnås, K. & Humlum, O. 2012: The relative age of mountain permafrost – estimation of Holocene permafrost limits in Norway. *Global and Planetary Change 92-93*, 209–223.

Linge, H., Brook, E. J., Nesje, A., Raisbeck, G. M., Yiou, F. & Clark, H. 2006: In situ [10]Be exposure ages from southeastern Norway: implications for the geometry of the Weichselian Scandinavian ice sheet. *Quaternary Science Reviews 25*, 1097–1109.

Linge, H., Nesje, A., Matthews, J. A., Fabel, D. & Xu, S. 2020: Evidence for rapid paraglacial formation of rock glaciers in southern Norway from [10]Be surface exposure dating. *Quaternary Research 97*, 44–70.

Lussana, C., Tveito, O. E., Dobler, A. & Tunheim, K. 2019: seNorge_2018, daily precipitation, and temperature datasets over Norway. *Earth System Science Data 11*, 1531–1551.

Lutro, O. & Tveten, E. 2012: *Berggrunnskart GALDHØPIGGEN 1518 II, 1:50,000*. Norges geologiske undersøkelse.

Lyså, A., Knies, J. & Larsen, E. 2008: Kunnskap om istider og landformer – nøkkelen til forståelsen av klimavariasjoner. *Gråsteinen 12*, 41–57.

Mangerud, J. 2023: Younger Dryas Stadial (YD) local moraines in western and northern Norway. *In* Palacios, D., Hughes, P. D., García-Ruiz, J. M. & Andrés, N. (eds.): *European Glacial Landscapes. The Last Deglaciation*, 453–466. Elsevier, Amsterdam.

Mangerud, J., Gyllencreutz, R., Lohne, Ø. & Svendsen, J. I. 2011: Glacial history of Norway. *In* Ehlers, J., Gibbard, P. L. & Hughes, P. D. (eds.): *Quaternary Glaciations – Extent and Chronology: A Closer Look*, 279–298. Elsevier, Amsterdam.

Mangerud, J., Hughes, A. L. C., Johnson, M. D. & Lunkka, J. P. 2023: The Fennoscandian Ice Sheet during the Younger Dryas Stadial. *In* Palacios, D., Hughes, P. D., García-Ruiz, J. M. & Andrés, N. (eds.): *European Glacial Landscapes. The Last Deglaciation*, 437–452. Elsevier, Amsterdam.

Marr, P., Winkler, S. & Löffler, J. 2019: Aspects of Late Weichselian deglaciation in South Norway: timing of deglaciation, ice sheet geometry, and climate variations inferred from surface exposure ages of Late Pleistocene and Holocene landforms. *Erdkunde 73*, 277–301.

Matthews, J. A. 1991: The late Neoglacial ('Little Ice Age') glacier maximum in southern Norway: new ^{14}C-dating evidence and climatic implications. *The Holocene 1*, 219–233.

Matthews, J. A. 2005: 'Little Ice Age' glacier variations in Jotunheimen, southern Norway: a study in regionally-controlled lichenometric dating of recessional moraines with implications for climate and lichen growth rates. *The Holocene 15*, 1–19.

Matthews, J. A. 2013: Neoglaciation in Europe. *In* Elias, S. A. (ed.): *Encyclopedia of Quaternary Science 2*, 257–268. Elsevier, Amsterdam.

Matthews, J. A. & Dresser, P. Q. 2008: Holocene glacier variation chronology of the Smørstabbtindan massif, Jotunheimen, Norway, and the recognition of European Neoglacial Events. *The Holocene 18*, 181–201.

Matthews, J. A. & Owen, G. 2010: Schmidt-hammer exposure-age dating: developing linear age-calibration curves using Holocenes bedrock surfaces from the Jotunheimen– Jostedalsbreen regions of southern Norway. *Boreas 39*, 105–115.

Matthews, J. A. & Owen, G. 2011: Holocene chemical weathering, surface lowering and rock weakening rates on glacially eroded bedrock surfaces in an alpine periglacial environment, Jotunheimen, Norway. *Permafrost and Periglacial Processes 22*, 279–290.

Matthews, J. A. & Winkler, S. 2022: Schmidt-hammer exposure-age dating (SHD): a review of principles and practice. *Earth-Science Reviews 230*, 104038, https://doi.org/10.1016/j.earscirev.2022.104038.

Matthews, J. A., Berrisford, M. S., Dresser, P. Q., Nesje, A., Dahl, S. O., Bjune, A. E., Bakke, J., Birks, J. H. B., Lie, Ø., Dumayne-Peaty, L. & Barnett, C. 2005: Holocene glacier history of Bjørnbreen and climatic reconstruction in central Jotunheimen, Norway, based on proximal glaciofluvial stream-bank mires. *Quaternary Science Reviews 24*, 67–90.

Matthews, J. A., Dahl, S. O., Nesje, A., Berrisford, M. S. & Andersson, C. 2000: Holocene glacier variations in central Jotunheimen, southern Norway based on distal glaciolacustrine sediment cores. *Quaternary Science Reviews 19*, 1625–1647.

Matthews, J. A., Hill, J. L., Winkler, S., Owen, G. & Vater, A. E. 2018: Autosuccession in alpine vegetation: testing the concept on an altitudinal bioclimatic gradient, Jotunheimen, southern Norway. *Catena 170*, 169–182.

Matthews, J. A., Wilson, P., Winkler, S., Mourne, R. W., Hill, J. L., Owen, G., Hiemstra, J. F., Hallang, H. & Geary, A. P. 2019: Age and development of active cryoplanation terraces in the alpine permafrost zone at Svartkampan, Jotunheimen, southern Norway. *Quaternary Research 92*, 641–664.

Matthews, J. A., Winkler, S. & Wilson, P. 2014: Age and origin of ice-cored moraines in Jotunheimen and Breheimen, southern Norway: insights from Schmidt-hammer exposure-age dating. *Geografiska Annaler Series A ( Physical Geography ) 96*, 531–548.

Meier, M. F. & Post, A. S. 1962: Recent variations in mass net budgets of glaciers in western North America. *Association Internationale d'Hydrologie Scientifique, Publication 58*, 63–77.

Meierding, T. C. 1982: Late Pleistocene glacial equilibrium line in the Colorado Front Range: a comparison of methods. *Quaternary Research 18*, 289–310.

Mekhaldi, F., Czymzik, M., Adolphi, F., Sjolte, J., Björck, S., Aldahan, A., Brauer, A., Martin-Puertas, C., Possnert, G. & Muscheler, R. 2020: Radionuclide wiggle matching reveals a nonsynchronous early Holocene climate oscillation in Greenland and western Europe around a grand solar minimum. *Climate of the Past 16*, 1145–1157.

Nesje, A. 1992: Topographic effects on the equilibrium-line altitude on glaciers. *GeoJournal 27*, 383–391.

Nesje, A. 2009: Late Pleistocene and Holocene alpine glacier fluctuations in Scandinavia. *Quaternary Science Reviews 28*, 2119–2136.

Nesje, A. & Dahl, S. O. 1991: Holocene glacier variations of Blåisen, Hardangerjøkulen, central southern Norway. *Quaternary Research 35*, 25–40.

Nesje, A. & Dahl, S. O. 1992: Equilibrium-line altitude depression of reconstructed Younger Dryas and Holocene glaciers in Fosdalen, inner Nordfjord, western Norway. *Norsk Geologisk Tidsskrift 72*, 209–216.

Nesje, A. & Dahl, S. O. 2001: The Greenland 8200 cal. yr BP event detected in loss-on-ignition profiles in Norwegian lacustrine sediment sequences. *Journal of Quaternary Science 16*, 155–166.

Nesje, A. & Matthews, J. A. 2023: Holocene glacial landscapes of the Scandinavian Peninsula. *In* Palacios, D., Hughes, P. D., Jomelli, V. & Tanarro, L. M. (eds.): *European Glacial Landscapes: The Holocene*, 245–274. Elsevier, Amsterdam.

Nesje, A., Kvamme, M., Rye, N. & Løvlie, R. 1991: Holocene glacial and climate history of the Jostedalsbreen region, western Norway; evidence from lake sediments and terrestrial deposits. *Quaternary Science Reviews 10*, 87–114.

Nicholson, D. T. 2009: Holocene microweathering rates and processes on ice-eroded bedrock, Røldal area, Hardangervidda, southern Norway. *In* Knight, J. & Harrison, S. (eds.): *Periglacial and Paraglacial Processes and Environments*, 29–49. *Geological Society, London, Special Publications 320*.

Nishiizumi, K. 2004: Preparation of $^{26}$Al AMS standards. *Nuclear Instruments and Methods in Physics Research B 223–224*, 388–392.

Nishiizumi, K., Imamura, M., Caffee, M. W., Southon, J. R., Finkel, R. C. & McAninch, J. 2007: Absolute calibration of $^{10}$Be standards. *Nuclear Instruments and Methods in Physics Research B 258*, 403–413.

Nydal, R., Løvseth, K. & Syrstad, O. 1970: Trondheim natural radiocarbon measurements V. *Radiocarbon 12*, 205–237.

Ødegård, R. S., Nesje, A., Isaksen, K., Andreassen, L. M., Eiken, T., Schwikowski, M. M. & Uglietti, C. 2017: Climate change threatens archaeologically significant ice patches: insights into their age, internal structure, mass balance and climate sensitivity. *The Cryosphere 11*, 17–32.

Ødegård, R. S., Sollid, J. L. & Liestøl, O. 1987: *Juvflya – Kvartærgeologi og geomorfologi M 1:10.000*. Geografisk Institutt, Universitetet i Oslo, Oslo.

Ødegård, R. S., Sollid, J. L. & Liestøl, O. 1988: Periglacial forms related to terrain parameters in Jotunheimen, southern Norway. *In* Senneset, K. (ed.): *5th International Conference on Permafrost, Proceedings, vol. 3*, 59–61. Tapir, Trondheim.

Ødegård, R. S., Sollid, J. L. & Liestøl, O. 1992: Ground temperature measurements in mountain permafrost, Jotunheimen, southern Norway. *Permafrost and Periglacial Processes 3*, 231–234.

Østrem, G. 1964: Ice-cored moraines in Scandinavia. *Geografiska Annaler 46*, 282–337.

Østrem, G. 1965: Problems of dating ice-cored moraines. *Geografiska Annaler 47*, 1–38.

Owen, G., Matthews, J. A. & Albert, P. G. 2007: Rates of Holocene chemical weathering, 'Little Ice Age' glacial erosion, and implications for Schmidt-hammer dating at a glacier-foreland boundary, Fåbergstølsbreen, southern Norway. *The Holocene 17*, 829–834.

Patton, H., Hubbard, A., Andreassen, K., Auriac, A., Whitehouse, P. L., Stroeven, A. P., Shackleton, C., Winsborrow, M., Heyman, J. & Hall, A. M. 2017: Deglaciation of the Eurasian ice sheet complex. *Quaternary Science Reviews 169*, 148–172.

Pellitero, R., Rea, B. R., Spagnola, M., Bakke, J., Ivo-Ochs, S., Hughes, P., Lukas, S. & Ribolini, A. 2015: A GIS tool for automatic calculation of glacier equilibrium-line altitudes. *Computers and Geosciences 82*, 55–62.

Peltier, W. R., Argus, D. F. & Drummond, R. 2015: Space geodesy constrains ice age terminal deglaciation: the global ICE-6G_C (VM5a) model. *Journal of Geophysical Research: Solid Earth 120*, 450–487.

Péwé, T. L. & Reger, R. D. 1972: Modern and Wisconsinan snowlines in Alaska. *Proceedings of the 24th International Geologic Congress 12*, 187–197.

Porter, S. C. 1975: Equilibrium-line altitudes of Late Quaternary glaciers in the Southern Alps, New Zealand. *Quaternary Research 5*, 27–47.

Proceq 2017: *Concrete Test Hammer ( "Original Schmidt" ). Operating Instructions*. 22 pp. Proceq, Schwerzenbach.

Rasmussen, S. O., Bigler, M., Blockley, S. P., Blunier, T., Buchardt, S. L., Clausen, H. B., Cvijanovic, I., Dahl-Jensen, D., Johnsen, S. J.,

Fischer, H., Gkinis, V., Guillevic, M., Hoek, W. Z., Lowe, J. J., Pedro, J. B., Popp, T., Seierstad, I. K., Steffensen, J. P., Svensson, A. M., Vallelonga, P., Vinther, B. M., Walker, M. J. C., Wheatley, J. J. & Winstrup, M. 2014: A stratigraphic framework for abrupt climatic changes during the Last Glacial period based on three synchronized Greenland ice-core records: refining and extending the INTIMATE event stratigraphy. *Quaternary Science Reviews 106*, 14–28.

Rasmussen, S. O., Vinther, B. M., Clausen, H. B. & Andersen, K. K. 2007: Early Holocene climate oscillations recorded in three Greenland ice cores. *Quaternary Science Reviews 26*, 1907–1914.

Rea, B. R. 2009: Defining modern day area-altitude balance ratios (AABRs) and their use in glacier-climate reconstructions. *Quaternary Science Reviews 28*, 237–248.

Reitner, J., Ivy-Ochs, S., Drescher-Schneider, R., Hajdas, I. & Linner, M. 2016: Reconsidering the current stratigraphy of the Alpine Lateglacial: implications of the sedimentary and morphological record of the Lienz area (Tyrol/Austria). *E&G Quaternary Science Journal 65*, 113–144.

Romundset, A., Akçar, N., Fredin, O., Andersen, J. L., Høgaas, F., Christl, M., Yesilyurt, S. & Schlüchter, C. 2023: Early Holocene thinning and final demise of the Scandinavian Ice Sheet across the main drainage divide of southern Norway. *Quaternary Science Reviews 317*, 108274, https://doi.org/10.1016/j.quascirev.2023.108274.

Shakesby, R. A., Matthews, J. A., Karlén, W. & Los, S. O. 2011: The Schmidt hammer as a Holocene calibrated-age dating technique: testing the form of the R-value-age relationship and defining the predicted-age errors. *The Holocene 21*, 615–628.

Shakesby, R. A., Matthews, J. A. & Owen, G. 2006: The Schmidt hammer as a relative age dating tool and its potential for calibrated-age dating in Holocene glacial environments. *Quaternary Science Reviews 25*, 2846–2867.

Shakesby, R. A., Matthews, J. A., Winkler, S., Fabel, D. & Dresser, P. Q. 2020: Early-Holocene moraine chronology, Sognefjell area, southern Norway: evidence for multiple glacial and climatic fluctuations within the Erdalen Event (~10.2-9.7 ka). *Norwegian Journal of Geology 100*, 20214, https://doi.org/10.17850/njg100-3-2.

Sollid, J. L. & Reite, A. 1983: The last glaciation and deglaciation of central southern Norway. *In* Ehlers, J. (ed.): *Glacial Deposits of North-West Europe*, 41–60. Balkema, Rotterdam.

Sollid, J. L. & Sørbel, L. 1981: *Kvartærgeologisk verneverdige områder i Midt-Norge. Rapport T-524.* 207 pp. Miljøverndepartementet, Avdeling for naturvern og friluftsliv, Oslo.

Sollid, J. L. & Sørbel, L. 1988: Influence of temperature conditions in formation of end moraines in Fennoscandia and Svalbard. *Boreas 17*, 553–558.

Sollid, J. L. & Sørbel, L. 1994: Distribution of glacial landforms in southern Norway in relation to the thermal regime of the last continental ice sheet. *Geografiska Annaler Series A (Physical Geography) 76A*, 25–35.

Stahl, T., Winkler, S., Quigley, M., Bebbington, M., Duffy, B. & Duke, D. 2013: Schmidt hammer exposure-age dating (SHD) of Late Quaternary fluvial terraces in New Zealand. *Earth Surface Processes and Landforms 38*, 1838–1850.

Stroeven, A. P., Hättestrand, C., Kleman, J., Heyman, J., Fabel, D., Fredin, O., Goodfellow, B. W., Harbor, J. M., Jansen, J. D., Olsen, L., Caffee, M. W., Fink, D., Lundqvist, J., Rosqvist, G. C., Stromberg, B. & Jansson, K. N. 2016: Deglaciation of Fennoscandia. *Quaternary Science Reviews 147*, 91–121.

Sumner, P. & Nel, W. 2002: The effect of rock moisture on Schmidt hammer rebound: tests on rock samples from Marion Island and South Africa. *Earth Surface Processes and Landforms 27*, 1137–1142.

Sutherland, D. G. 1984: Modern glacier characteristics as a basis for inferring former climates with particular reference to the Loch Lomond Stadial. *Quaternary Science Reviews 3*, 291–309.

Tomkins, M. D., Dortch, J. M. & Hughes, P. D. 2016: Schmidt Hammer exposure dating (SHED): establishment and implications for the retreat of the last British Ice Sheet. *Quaternary Geochronology 33*, 46–60.

Tomkins, M. D., Dortch, J. M., Hughes, P. D., Huck, J. J., Stimson, A. G., Delmas, M., Calvet, M. & Pallàs, R. 2018a: Schmidt hammer exposure dating (SHED): rapid age assessment of glacial landforms in the Pyrenees. *Quaternary Research 90*, 26–37.

Tomkins, M. D., Huck, J. J., Dortch, J. M., Hughes, P. D., Kirkbride, M. P. & Barr, I. D. 2018b: Schmidt hammer exposure age dating (SHED): calibration procedures, new exposure age data and an online calculator. *Quaternary Geochronology 44*, 55–62.

Velle, G., Bjune, A. E., Larsen, J. & Birks, H. J. B. 2010: Holocene climate and environmental history of Brurskardtjørni, a lake in the catchment of Øvre Heimdalsvatn, south-central Norway. *Hydrobiologia 642*, 13–34.

Vermeesch, P. 2007: CosmoCalc: an Excel add-in for cosmogenic nuclide calculations. *Geochemistry, Geophysics, Geosystems 8*, Q08003, https://doi.org/10.1029/2006GC001530.

Vinther, B. M., Clausen, H. B., Johnson, S. J., Rasmussen, S. O., Andersen, K. K., Buchard, S. L., Dahl-Jensen, D., Seierstad, I. K., Siggaard-Andersen, M.-L., Steffensen, J. P. & Svensson, A. 2006: A synchronized dating of three Greenland ice cores throughout the Holocene. *Journal of Geophysical Research 111*, D13102, https://doi.org/10.1029/2005JD006921.

Vorren, T. O. & Mangerud, J. 2008: Glaciations come and go. Pleistocene, 2.6 million–11,500 years ago. *In* Ramberg, I., Bryhni, I., Nøttvedt, A. & Rangnes, K. (eds.): *The Making of a Land – Geology of Norway*, 480–533. Geological Society of Norway, Trondheim.

Vorren, T. O., Mangerud, J., Blikra, L. H., Nesje, A. & Sveian, H. 2008: The emergence of modern Norway. The last 11,500 years – the Holocene. *In* Ramberg, I. B., Bryhni, I., Nøttvedt, A. & Rangnes, K. (eds.): *The Making of a Land – Geology of Norway*, 534–559. Geological Society of Norway, Trondheim.

Winkler, S., Donner, A. & Tintrup gen Suntrup, A. 2021: Periglacial landforms in Jotunheimen, central southern Norway, and their altitudinal distribution. *In* Beylich, A. A. (ed.): *Landscapes and Landforms of Norway*, 169–202. Springer, Berlin.

Winkler, S., Matthews, J. A., Haselberger, S., Hill, J. L., Mourne, R. W., Owen, G. & Wilson, P. 2020: Schmidt-hammer exposure-age dating (SHD) of sorted stripes on Juvflye, Jotunheimen (central South Norway): morphodynamic and palaeoclimatic implications. *Geomorphology 353*, 107014, https://doi.org/10.1016/j.geomorph.2019.107014.

Winkler, S., Matthews, J. A., Mourne, R. W. & Wilson, P. 2016: Schmidt-hammer exposure ages from periglacial patterned ground (sorted circles) in Jotunheimen, Norway, and their interpretative problems. *Geografiska Annaler: Series A (Physical Geography) 98*, 265–285.

## Supporting Information

Additional Supporting Information to this article is available at http://www.boreas.dk.

*Fig. S1*. Topographic map (A) and corresponding aerial image (B) for the site near Galdhøpiggen. The geomorphological setting and periglacial features in the vicinity of the moraines are indicated on the aerial image. The moraine fragments (dark green) central in this study are located in the northern slope of Juvvasshøe. Aerial images show a gradual change from an area of predominantly periglacial patterned ground (sorted circles and stripes; violet), to an area dominated by solifluction lobes with clear surface stripes (striped solifluction lobes; purple), to solifluction lobes with uniform (vegetated) surface characteristics (solifluction lobes, maroon). The eastern part of the site is dominated of temporal snowbeds (white), with snow patches and/or no/restricted lichen growth. The ice-cored moraine in the southwestern corner is a Little Ice Age feature formed by the glacier in Kjelen, west of Lake Juvvatnet. The map and aerial image were

retrieved via Kartverket (https://norgeskart.no and https://norgeibilder.no). Figure S3A was partly used to outline the landform setting.

*Fig. S2*. Topographic map (A) and corresponding aerial image (B) for the site near Glittertinden. The geomorphological setting and periglacial features in the vicinity of the moraines are indicated on the aerial image. The moraine fragments (dark green) central in this study are located on the western side of the Bergenussa river. Dotted moraine fragments have only been briefly checked in the field. The aerial image predominantly shows an area of periglacial patterned ground (sorted circles and stripes; violet), and a smaller area dominated by solifluction lobes with uniform (vegetated) surface characteristics (solifluction lobes; maroon). Lateral meltwater channels are cut by the younger marginal moraine fragments. The ice-cored moraine in the southwestern corner is a Little Ice Age feature formed by the Gråsubreen glacier. The map and aerial image were retrieved via Kartverket (https://norgeskart.no and https://norgeibilder.no). Figure S3B was to a large degree used to outline the landform setting.

*Fig. S3*. Digital elevation models for the area outlined in Fig. 3A near Galdhøpiggen (A) and the area near Glittertinden in Fig. 3B (B), retrieved from Kartverket (https://hoydedata.no/).

*Fig. S4.1*. Sample JUV 1901. Photos of (A) surface after sampling (hammer length 28.5 cm; hammer head 4 × 4 × 9 cm), (B) the field setting (sitting people for scale, white arrow marks sampled boulder), (C) the sample material before crushing (A3 sheet (29.7 × 42.0 cm) with tape marking) and (D) sampled material consisting mainly of coarse-grained quartz, feldspar, garnet and muscovite.

*Fig. S4.2*. Sample JUV 1902. Photos of (A) the surface before sampling (yellow/black try-square tool 13 × 20.5 cm), (B) the field setting (standing people for scale, white arrow marks sampled boulder), (C) the sample material before crushing (A3 sheet (29.7 × 42.0 cm) with tape marking) and (D) the sampled material consisting mainly of coarse-grained quartz, feldspar, garnet, muscovite, biotite and gneiss xenolith.

*Fig. S4.3*. Sample JUV 1903. Photos of (A) the surface before sampling (hammer length 28.5 cm; hammer head 4 × 4 × 9 cm), (B) the field setting (sitting people for scale, white arrow marks sampled boulder), (C) the sample material before crushing (A3 sheet (29.7 × 42.0 cm) with tape marking) and (D) the

sampled material consisting mainly of fine-grained quartz, feldspar and muscovite.

*Fig. S4.4*. Sample JUV 1905. Photos of (A) the surface before sampling (hammer length 28.5 cm; hammer head 4 × 4 × 9 cm), (B) the field setting (sitting people for scale, white arrow marks sampled boulder), (C) the sample material before crushing (A3 sheet (29.7 × 42.0 cm) with tape marking) and (D) the sampled material consisting mainly of fine-grained quartz, feldspar, biotite, hornblende and muscovite.

*Fig. S4.5*. Sample JUV 1906. Photos of (A) the surface before sampling (hammer length 28.5 cm; hammer head 4 × 4 × 9 cm), (B) the field setting (standing person for scale, white arrow marks sampled boulder), (C) the sample material before crushing (A3 sheet (29.7 × 42.0 cm) with tape marking) and (D) the sampled material consisting mainly of medium-grained quartz, feldspar, biotite and hornblende.

*Fig. S4.6*. Sample JUV 1907. Photos of (A) the surface before sampling (yellow/black try-square tool 13 × 20.5 cm), (B) the field setting (standing people for scale, white arrow marks sampled boulder), (C) the sample material before crushing (A3 sheet (29.7 × 42.0 cm) with tape marking) (D) the sampled material consists mainly of coarse-grained quartz, feldspar, biotite and muscovite.

*Fig. S4.7*. Sample JUV 1908. Photos of (A) the surface before sampling (hammer: length 28.5 cm, head 4 × 4 × 9 cm, yellow arrow marks crack/fissure), (B) the field setting (standing people for scale, white arrow marks sampled boulder), (C) the sample material before crushing (A3 sheet (29.7 × 42.0 cm) with tape marking) and (D) the sampled material consists mainly of fine-grained quartz, feldspar and mica.

*Fig. S4.8*. Sample JUV 1909. Photos of (A) the surface after sampling (fat chisel 18.5 cm long), (B) the field setting (people for scale, white arrow marks sampled boulder), (C) the sample material before crushing (A3 sheet (29.7 × 42.0 cm) with tape marking) and (D) the sampled material consisting mainly of medium- to coarse-grained quartz, feldspar, biotite, and hornblende.

*Fig. S4.9*. Sample JUV 1910. Photos of (A) the surface before sampling (hammer: length 28.5 cm, head 4 × 4 × 9 cm), (B) the field setting (people for scale, white arrow marks sampled boulder, red-border arrow marks JUV 1909), (C) the sample material before crushing (A3 sheet (29.7 × 42.0 cm) with tape marking) and (D) the sampled material consisting mainly of

medium- to coarse-grained quartz, feldspar and biotite.

*Fig. S4.10.* Sample JUV 1911. Photos of (A) the surface after sampling (hammer: length 28.5 cm, head 4 × 4 × 9 cm), (B) the field setting (people for scale, white arrow marks sampled boulder, red-border arrow marks JUV 1909), (C) the sample material before crushing (A3 sheet (29.7 × 42.0 cm) with tape marking) and (D) the sampled material consisting mainly of medium- to coarse-grained quartz, feldspar and biotite.

*Fig. S4.11.* Sample JUV 2201. Photos of (A) the surface after sampling (hammer: length 28.5 cm, head 4 × 4 × 9 cm), (B) the field setting (people for scale, white arrow marks sampled boulder), (C) the sample material before crushing (A3 sheet (29.7 × 42.0 cm) with tape marking) and (D) the sampled material consisting mainly of medium-grained quartz and feldspar.

*Fig. S4.12.* Sample BER 2101. Photos of (A) the surface after sampling (hammer: length 28.5 cm, head 4 × 4 × 9 cm), (B) the field setting (white arrow marks sampled boulder), (C) the outer surface of sample material before crushing (A3 sheet (29.7 × 42.0 cm) with tape marking) and (D) the inner surface of sample material before crushing. The sampled material consists mainly of medium-grained quartz and feldspar.

*Fig. S4.13.* Sample BER 2102. Photos of (A) the surface after sampling, (B) the field setting (standing hound for scale), (C) the outer surface of sample material before crushing (A3 sheet (29.7 × 42.0 cm) with tape marking) and (D) the inner surface of sample material before crushing. The sampled material consists mainly of medium-grained quartz and feldspar.

*Fig. S4.14.* Sample BER 2103. Photos of (A) the surface after sampling (black hand-held GPS Garmin Montana 680t for scale), (B) the field setting (backpack to the right for scale, white arrow marks sampled boulder), (C) the outer surface of sample material before crushing (A3 sheet (29.7 × 42.0 cm) with tape marking) and (D) the inner surface of sample material before crushing. The sampled material consists mainly of medium-grained quartz and feldspar.

*Fig. S4.15.* Sample BER 2104. Photos of (A) the surface after sampling (open field book and hound for scale), (B) the field setting (backpack to the left for scale, white arrow marks sampled boulder), (C) the outer surface of sample material before crushing (A3 sheet

(29.7 × 42.0 cm) with tape marking) and (D) fine-grained lithology dominated by quartz and feldspar.

*Fig. S4.16.* Sample BER 2105. Photos of (A) the surface after sampling (black hand-held GPS Garmin Montana 680t for scale), (B) the field setting (backpack to the left for scale, white arrow marks sampled boulder), (C) the outer surface of sample material before crushing (A3 sheet (29.7 × 42.0 cm) with tape marking) and (D) the inner surface of sample material before crushing. Sampled material consists mainly of medium-grained quartz and feldspar.

*Fig. S4.17.* Sample BER 2201. Photos of (A) the surface after sampling (hammer: length 28.5 cm, head 4 × 4 × 9 cm), (B) the field setting (white arrow marks sampled boulder, red-border arrow marks BER 2202), (C) the outer surface of sample material before crushing (A3 sheet (29.7 × 42.0 cm) with tape marking) and (D) the medium- to fine-grained lithology dominated by quartz, feldspar, mica and garnet.

*Fig. S4.18.* Sample BER 2202. Photos of (A) the surface after sampling (hammer: length 28.5 cm, head 4 × 4 × 9 cm), (B) the field setting (white arrow marks sampled boulder, red-border arrow marks BER 2201), (C) the outer surface of sample material before crushing (A3 sheet (29.7 × 42.0 cm) with tape marking) and (D) the medium- to fine-grained lithology dominated by quartz, feldspar and mica.

*Fig. S4.19.* Sample BER 2203. Photos of (A) the surface after sampling (yellow/black try-square tool 13 × 20.5 cm), (B) the field setting (white arrow marks sampled boulder), (C) the outer surface of sample material before crushing (A3 sheet (29.7 × 42.0 cm) with tape marking) and (D) the fine-grained lithology dominated by quartz, feldspar and mica.

*Fig. S4.20.* Sample BER 2204. Photos of (A) the surface after sampling (hammer: length 28.5 cm, head 4 × 4 × 9 cm), (B) the field setting (white arrow marks sampled boulder), (C) the outer surface of sample material before crushing (A3 sheet (29.7 × 42.0 cm) with tape marking) and (D) the fine-grained lithology dominated by quartz, feldspar and mica.

*Fig. S4.21.* Sample BER 2205. Photos of (A) the surface before sampling (yellow/black try-square tool 13 × 20.5 cm), (B) the field setting (white arrow marks sampled bedrock surface), (C) the outer surface of sample material before crushing (A3 sheet (29.7 × 42.0 cm) with tape marking) and (D) the

fine-grained lithology dominated by quartz, feldspar, mica and garnet.

*Fig. S4.22*. Sample BER 2206. Photos of (A) the surface before sampling (yellow/black try-square tool 13 × 20.5 cm), (B) the field setting (standing hound for scale, white arrow marks sampled bedrock surface), (C) the outer surface of sample material before crushing (A3 sheet (29.7 × 42.0 cm) with tape marking) and (D) the fine-grained lithology dominated by quartz, feldspar and mica.

*Fig. S4.23*. Sample BRU 2201. Photos of (A) the surface before sampling (yellow/black try-square tool 13 × 20.5 cm), (B) the field setting (white arrow marks sampled bedrock surface), (C) the outer surface of sample material before crushing (A3 sheet (29.7 × 42.0 cm) with tape marking) and (D) the sampled material consisting mainly of quartz.

*Fig. S5*. Typical observations of weathering reliefs used for erosion rate assessment. (A) Gneiss boulder with a quartz vein protruding ca. 2 cm above the rock surface. (B) Gneiss boulder with quartz knobs protruding 1–1.5 cm above the rock surface. (C) Boulder surface showing granular disintegration, enhanced by crustose lichens, resulting in a pitted surface. (D) Boulder surface showing small-scale exfoliation (1–2 mm thick).

*Fig. S6*. Kernel density estimates for calculated ('raw') [10]Be ages from (A) Galdhøpiggen–Juvvasshøe ($n = 11$), and (B) Glittertinden–Bergenussa ($n = 11$). No corrections for erosion, snow shielding or glacio-isostatic uplift. Individual (lines) and summed (shaded) [10]Be ages (with their internal uncertainties) calculated with free MATLAB code from Balco (2001)

available from http://depts.washington.edu/cosmolab/pubs/gb_pubs/camelplot.m.

*Table S1*. Mean monthly and mean annual air temperature, precipitation and snow thickness for the sampled elevations at Galdhøpiggen and Glittertinden. Modelled data are retrieved from SeNorge (http://www.senorge.no).

*Table S2*. Description of surfaces sampled for [10]Be surface exposure dating.

*Table S3*. Summary of sample preparation protocol for surface exposure dating using *in situ* [10]Be.

*Table S4*. [10]Be mean ages computed using three different [10]Be production rates and two different scaling schemes. 'Calculated' infers ages calculated with no correction for erosion, snow shielding or glacio-isostatic uplift. 'Erosion, snow corrected' infers ages corrected for erosion (1.5 mm ka[−1]) and snow shielding (25% of modern (1958–2020) annual snow cover). 'Erosion, snow, uplift corrected' infers ages corrected for erosion and snow shielding (as described), and uplift. '*n*' infers number of samples included in the mean, '*' notifies that outliers have been excluded.

*Data S1*. Description of laboratory preparation.

*Data S2*. Description of AMS analysis of Be.

*Data S3*. Description of calculation and correction of [10]Be ages.

*Data S4*. References.